

Authors are grateful to an anonymous referee for helpful and thoughtful comments. Each comment is addressed individually below. The referee comments are recorded in normal type, and our responses are described in boldface type.

Atmos. Chem. Phys. Discuss., 12, C10589-C10590, 2012

www.atmos-chem-phys-discuss.net/12/C10589/2012/

© Author(s) 2012. This work is distributed under

the Creative Commons Attribute 3.0 License.

Interactive comment on “Atmospheric column-averaged mole fractions of carbon dioxide at 53 aircraft measurement sites” by Y. Miyamoto et al.

Anonymous Referee #1

Received and published: 14 December 2012

Review of “Atmospheric column-averaged mole fraction of carbon dioxide at 53 aircraft sites” by Miyamoto et al.

Miyamoto et al describe the integration of numerous aircraft profiles of CO₂ along with estimates of CO₂ above the aircraft ceiling to estimate XCO₂. Such a catalog of XCO₂ estimates is useful for evaluating XCO₂ data from GOSAT and SCIAMACHY.

I recommend publication of this study after the following additional scope is considered.

1. The age-of-air method for estimating stratospheric CO₂ should be more fully evaluated. Numerous profiles of HF, N₂O, etc are publically available from ACE-FTS for example that could provide a method for evaluating this approach beyond the few SF₆ profiles described. In addition, XHF measurements are publically available from NDAAC and TCCON that could be used to evaluate the approach.

We used the modeled age of air obtained by ACTM and it was evaluated and corrected by vertical profiles of SF₆ measured at 6 sites over 71 ° N – 90 ° S in the period of 1999 – 2006 (Patra et al., 2009). As described by Stiller et al. (2012), the two tracers that have been used most widely to derive

mean age are carbon dioxide (CO₂) and sulfur hexafluoride (SF₆). CO₂ has a seasonal cycle in the troposphere which can propagate into the stratosphere and makes the determination of mean age values below 2 yr ambiguous. On the other hand, SF₆ increases monotonically but with small interannual variability in the troposphere. Although some papers have discussed that the existence of its sink in the mesosphere can cause an artifact when dating old air (e.g., Waugh and Hall, 2002), Stiller et al. (2012) showed zonal mean distribution of air age derived by 10⁶ SF₆ vertical profiles from MIPAS measurements and concluded that the impacts of mesospheric SF₆-depleted air masses on the age of air distribution and its linear increase are small. Moreover, we compared the CO₂ profiles derived from the age of air with balloon-borne CO₂ measurements over Japan from 1987 to 2007 and corrected the SF₆ model ages. We think that our evaluation using SF₆ and correction with the balloon-borne CO₂ profiles would be no problem in our study. Although referee's ideas are interesting, we think that they would be out of scope in our paper. If we have a chance, we would like to evaluate with them as a future work.

2. Given that several of the aircraft sites have co-located TCCON instruments, a comparison of the XCO₂ presented in this study should be undertaken.

Thank you very much for your useful suggestion. We compared aircraft-based XCO₂ at NRT, SYD, LEF, and SGP with TCCON XCO₂ at Tsukuba, Wollongong, Park Falls, and Lamont, respectively. TCCON XCO₂ data were averaged within ± 30 minutes of GOSAT overpass time because they were originally prepared for validation of the GOSAT products. Then, aircraft-based XCO₂ data at each site were compared with TCCON XCO₂ on the same day as aircraft measurement. Figure R1-1 shows the scatter diagram of TCCON XCO₂ and aircraft-based XCO₂ at 4 observation sites. The averages of the differences (aircraft minus TCCON) and the 1 standard deviations were 0.00 ± 1.10 ppm at NRT and -1.56 ± 0.92 ppm at LEF (Table R1-1). The correlation coefficient and average of the differences between both datasets are 0.94 (with statistical

significance at the 99% level) and -0.10 ± 1.10 ppm at all sites, respectively. Thus, we found that aircraft-based XCO₂ data at several observation sites were in good agreement with co-located TCCON data. This result is very interesting and we think we may submit this as separated paper.

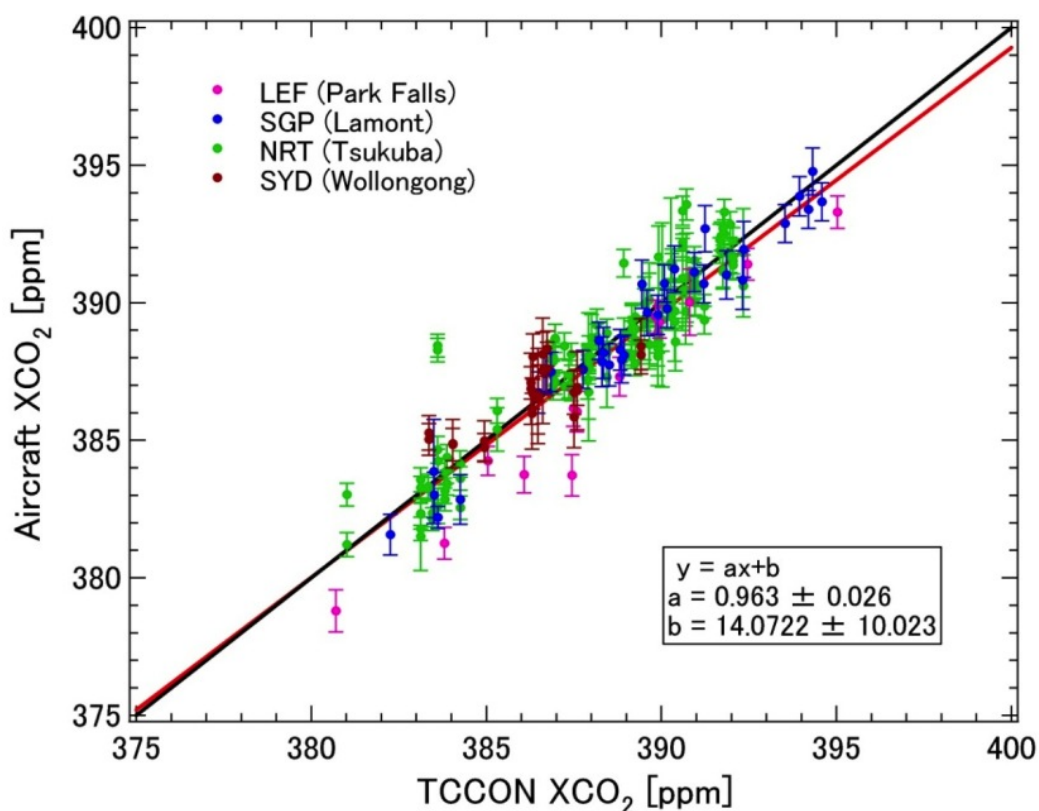


Figure R1-1. Scatter diagram between aircraft-based XCO₂ and TCCON XCO₂ on the same day as aircraft measurement at each observation site. Red line denotes the regression line based on all data. The one-to-one line is plotted as a black line.

Table R1-1. The average, 1 standard deviation (1σ), maximum and minimum of the differences, and the correlation coefficient (R) between aircraft-based XCO₂ and TCCON XCO₂ at each observation site.

	LEF (Park Falls)	SGP (Lamont)	NRT (Tsukuba)	SYD (Wollongong)	All sites
Number of dataset	13	33	132	24	202
R	0.98	0.98	0.93	0.77	0.94
average [ppm]	-1.56	-0.22	0.00	0.29	-0.10
1σ [ppm]	0.92	0.75	1.10	1.01	1.10
maximum [ppm]	-0.34	1.44	4.83	1.91	4.83
minimum [ppm]	-3.73	-1.50	-1.87	-1.65	-3.73

3. Because these profiles and associated estimates of XCO₂ will be broadly useful to the community, I suggest that they be organized and made publically available. A link to such a database would be helpful.

When comparing XCO₂ derived from the satellite measurements such as GOSAT with the aircraft measurements, column averaging kernels (CAKs) of the satellite measurements should be taken into account. Although much attention needs to be paid to using our XCO₂ dataset since it is not calculated with consideration of CAKs, it is very useful within the scientific community. Therefore, we would like to provide it on request.

We added above sentences before the last sentence of the second paragraph in Sect. 5 Conclusions.

Minor point.

Figure 4 is very difficult to read. I suggest the authors consider showing just a few of these panels (larger format) as examples and put the rest in a supplement or appendix.

We chose typical 7 sites and enlarged graphs for these sites were shown in Fig. 4. All results were placed in Supplementary materials. We also exchange open circles representing XCO₂ for closed circles and the corresponding text and caption were rewritten. We hope that new Fig. 4 looks better.

References

- Patra, P. K., Takigawa, M., Dutton, G. S., Uhse, K., Ishijima, K., Lintner, B. R., Miyazaki, K., and Elkins, J. W.: Transport mechanisms for synoptic, seasonal and interannual SF₆ variations and "age" of air in troposphere, *Atmos. Chem. Phys.*, 9, 1209-1225, 2009.
- Stiller, G. P., von Clarmann, T., Haenel, F., Funke, B., Glatthor, N., Grabowski, U., Kellmann, S., Kiefer, M., Linden, A., Lossow, S., and López-Puertas, M.: Observed temporal evolution of global mean age of stratospheric air for the 2002 to 2010 period, *Atmos. Chem. Phys.*, 12, 3311-3331, doi:10.5194/acp-12-3311-2012, 2012.
- Waugh, D. W. and Hall, T. M.: Age of stratospheric air: theory, observations, and models, *Rev. Geophys.*, 40, 1010, doi:10.1029/2000RG000101, 2002.

Atmospheric column-averaged mole fractions of carbon dioxide at 53 aircraft measurement sites

Y. Miyamoto^{1,*}, M. Inoue¹, I. Morino¹, O. Uchino¹, T. Yokota¹, T. Machida¹, Y. Sawa²,
H. Matsueda², C. Sweeney³, P. P. Tans³, A. E. Andrews³, P. K. Patra⁴

[1]{National Institute for Environmental Studies (NIES), Tsukuba, Japan}

[2]{Meteorological Research Institute (MRI), Tsukuba, Japan}

[3]{National Oceanic and Atmospheric Administration (NOAA), Boulder, Colorado, U.S.A.}

[4]{Japan Agency for Marine-Earth Science and Technology (JAMSTEC), Yokohama, Japan}

[*]{now at: Graduate School of Natural Science and Technology, Okayama University,
Okayama, Japan}

Correspondence to: I. Morino (morino@nies.go.jp)

Abstract

Atmospheric column-averaged mole fractions of carbon dioxide (X_{CO_2}) at 53 locations around the world were derived from aircraft measurements covering the altitude range of about 1-10 km. We used CO_2 vertical profile measurements from three major carbon cycle programs, a global climatological data set of air number density profiles and tropopause height for calculating X_{CO_2} for the period of 2007-2009. Vertical profiles of the CO_2 mixing ratio are complemented by tall tower data up to 400 m from the earth's surface and by simulated profiles in the stratosphere from a chemistry-transport model. The amplitude of the

seasonal cycle of calculated XCO₂ values shows clear latitudinal dependence, and the amplitude decreases from about 10 ppm at high latitudes in the Northern Hemisphere to at most 2 ppm in the tropics and the Southern Hemisphere. The uncertainties of XCO₂ were estimated from assumptions about CO₂ profiles for each flight. Typically, uncertainties were less than 1 ppm; thus, this data set is within the level of uncertainty needed for primary validation of XCO₂ measurements by the Greenhouse gases Observing SATellite (GOSAT) and by future satellite missions for monitoring greenhouse gases.

1 Introduction

Atmospheric abundance of CO₂ has drawn great interest in the recent decade because CO₂ is the most important anthropogenically produced greenhouse gas (WMO, 2006). The Greenhouse gases Observing SATellite (GOSAT), launched on 23 January 2009, is equipped with a Fourier transform spectrometer (FTS) to observe the atmospheric column-averaged mole fraction of CO₂ (XCO₂) at more uniform geographical coverage than the in situ measurement network (WDCGG, 2012). GOSAT overpasses the region from 80°S to 80°N in longitudinal bands every 3 days. From 4 April 2009 to 31 July 2010, observational points were ~158 km apart cross-track and ~152 km apart along-track at the equator with the 5 point cross-track scan mode, and since 1 August 2010, observational points are ~263 km apart cross-track and ~283 km apart along-track at the equator with the 3 point cross-track scan mode (Yokota et al., 2009; Kuze et al., 2009; Yoshida et al., 2011). In contrast, the in situ measurement network comprised ~~of~~ fewer than 216 sites (WDCGG, accessed 10 October 2012). XCO₂ measurements by remote sensing ~~equipments~~ will provide another perspective for studying ~~the~~ carbon cycle processes by better constraining the surface fluxes through inverse modeling. Modeling studies have shown that uncertainty of the source/sink inversion

1 results is linked to the error of the satellite CO₂ measurements (e.g., Rayner et al., 2002; Patra
2 et al., 2003). Miller et al. (2007) showed that precisions of 1–2 ppm in XCO₂ satellite
3 measurements are needed to improve our knowledge of carbon cycle phenomena. Therefore,
4 it is important to evaluate the quality of data obtained from satellites by comparing them with
5 more accurate, though sparse, in situ observations.

6 Because of their high accuracy, aircraft profile measurements are used for comparison with
7 satellite data, but these measurements are limited in frequency and spatial density. Recently,
8 the CONTRAIL (Comprehensive Observation Network for TRace gases by AirLiner) project,
9 by using commercial airplanes, has succeeded in measuring frequent and vertically dense data
10 over a number of airports (Machida et al., 2008). CO₂ mixing ratios recorded during takeoff
11 and landing can be used to calculate XCO₂ above airports.

12 Another XCO₂ data set useful for validating satellite data is from the Total Carbon Column
13 Observing Network (TCCON, Wunch et al., 2010, 2011a, 2011b; Morino et al., 2011;
14 Schneising et al., 2012), a ground-based FTS network. The measurement uncertainty of the
15 FTS system, which has been certified by aircraft measurements, is similar to that of them, and
16 the FTS network covers a wider area, but the number of aircraft measurements sites are
17 greater than that of the TCCON sites.

18 Araki et al. (2010) reported XCO₂ values calculated over Tsukuba, Japan, from CONTRAIL
19 data obtained at Narita Airport and ancillary data sets. They also estimated the uncertainty
20 derived from the assumptions made about the air density profile, the tropopause height, and
21 the CO₂ profile near the surface.

22 In this study, we report the results of XCO₂ calculations carried out with data provided by
23 CONTRAIL, measurements made by the U.S. National Oceanic and Atmospheric
24 Administration (NOAA) and the National Institute for Environmental Studies (NIES), Japan

at 53 sites between 2007 and 2009. The method used in this study is similar to that of Araki et al. (2010), but the treatment of the stratospheric vertical profile has been improved. Section 2 briefly describes the measurements by CONTRAIL, NOAA, and NIES. Section 3 presents details of the calculation of XCO₂ and estimation of its uncertainty. In Section 4, the results of the calculation of XCO₂ temporal behavior are presented and their uncertainties are discussed.

2 Observations

Aircraft measurements obtained by CONTRAIL, NOAA, and NIES between 2007 and 2009 were used in this study. Details of each project have been reported elsewhere (Machida et al., 2008; Machida et al., 2001; Tans et al., 1996; ESRL/GMD CCGG Aircraft Program, 2011) and are only described briefly here. The locations of the CONTRAIL, NOAA, and NIES observations are shown in Fig. 1, and they are listed along with their three-letter site codes in Table 1.

The CONTRAIL project takes advantage of the numerous flights made by commercial airlines worldwide to acquire frequent measurements of CO₂ at a relatively large number of sites. Automatic air sampling equipment for discrete sampling and continuous CO₂ measuring equipment (CME) for *in situ* observations are installed onboard aircraft operated by Japan Airlines. XCO₂ is calculated from the data obtained by CME upon departure from and arrival at 28 different airports. These profiles differ from those obtained by the NOAA and NIES aircraft because the commercial aircraft move horizontally over a few hundred kilometers during their takeoff and landing. The data are typically collected at altitudes between a few kilometers and 10 km (Machida et al., 2008). Measurements are not carried out at regular time intervals at all locations. For example, there were 10 flights in May 2007 and only 2 flights in April 2007 at Schiphol Airport (AMS, Amsterdam, the Netherlands). The CME observations

are calibrated onboard the airplane with standard gases based on NIES 09 CO₂ scale, which is close to World Meteorological Organization (WMO) standards (Machida et al., 2011) at 10 min intervals during ascending and descending and at 40 min intervals during cruising. The uncertainty of the CME observations is estimated to be about 0.2 ppm (Machida et al., 2008).

The NOAA measurements are from an aircraft observation network of 21 sites operated by the Global Monitoring Division of the Earth System Research Laboratory (GMD/ESRL). Flask sampling observations are performed several times a month, and the reported uncertainty is ~0.15 ppm. The typical altitude range is from a few hundred meters to 5–8 km above ground level (ESRL/GMD CCGG Aircraft Program, 2011; <http://www.esrl.noaa.gov/gmd/ccgg/aircraft/index.html>).

The measurements by NIES are made by flask sampling at three sites in Russia and one site in Japan. Sampling frequency is once or twice a month. Typical observing altitudes are 0.5–7 km. The uncertainty is estimated to be 0.2 ppm, which takes into account the scale difference between standard gases (Machida et al., 2001).

3 Method

The calculation method used in this study is basically equivalent to that used by Araki et al. (2010) in their analysis, with the following modifications, mainly to make the method applicable to places anywhere in the world.

The vertical profiles of the CO₂ mixing ratios in dry air are calculated from aircraft measurements made over a limited altitudinal range. Therefore, to calculate XCO₂, additional information is needed: (1) supplemental vertical profiles of CO₂ in the altitude range where observation data are not available, and (2) vertical profiles of the dry air number density above the sites. In this study, similar to Araki et al. (2010), these two types of profiles (CO₂

1 mixing ratio and the dry air number density) were prepared from ground level to 85 km above
2 the ground.

3 To construct stratospheric profiles, Araki et al. (2010) used an empirical model of CO₂
4 profiles at mid-latitudes in the Northern Hemisphere. In this model, the concentration is
5 assumed to be constant above 20 km and values between the tropopause and 20 km are
6 obtained by linear interpolation. In this study, profiles derived from the modeled “age of air”
7 were used to calculate XCO₂ at various latitudes. The age of air was obtained from
8 simulations by the atmospheric general circulation model-based chemistry-transport model
9 (ACTM) of the NIES/Center for Climate System Research/Frontier Research Center for
10 Global Change (Patra et al., 2009). The modeled age of air was compared with ages estimated
11 by using several vertical profiles of sulfur hexafluoride (SF₆) in the upper troposphere and
12 stratosphere in the latitude range of 17–70°N, based on measurements made by balloon-borne
13 instruments (Harnisch et al., 1996; Patra et al., 1997), to obtain correction factors at each
14 profile location. The correction factors at each profile location were then interpolated and
15 applied to all model grid cells between the equator and the North Pole. The mirror image was
16 used for the Southern Hemisphere under the assumption that the age of air in the stratosphere
17 is determined by vertical mixing at the equator (e.g., Andrews et al., 2001; Austin and Li,
18 2006). The ages were converted to CO₂ mixing ratios by assuming that the tropospheric
19 concentration (corresponding to 0-year-old mixing ratio) in 2006 was 381.2 ppm and that the
20 annual increasing trend was 1.9 ppm/year at every site (WMO, 2006). This study estimated
21 the mean age to be about 5–6 years in the mid-latitude stratosphere (24–50 km). This result is
22 consistent with the findings of other recent studies on the age of stratospheric air (e.g.,
23 Ishidoya et al., 2008; Engel et al., 2009). Zhu et al. (2000) showed that the mean age of air is
24 about 6.5 years even at 80 km by using a globally balanced two-dimensional middle
25 atmosphere model. The amount of CO₂ above 50 km is so small that assumptions about the

1 profile above 50 km do not affect the results within the uncertainties. Therefore, the modeled
2 profile was used up to 50 km, and above 50 km the mixing ratio was assumed to be constant
3 at the 50-km value. The CO₂ profiles derived from the age of air have been compared with
4 measurements of CO₂ made by balloon-borne instruments over Japan from 1987 to 2007 at
5 Sanriku (39.1°N, 141.8°E) (Nakazawa et al., 1995). These data show an increasing trend of
6 1.52 ppm/year, so all data were normalized to 1 January 2007 using this value. The trend
7 obtained at Sanriku differs from the world-average trend of 1.9 ppm/year in 2000's because it
8 was determined by data collected over a different period (1996–2005). The normalized data
9 were averaged within each altitude range: 15–20, 20–25, 25–30, and above 30 km. The
10 uncorrected model clearly underestimated the age of air at most heights, particularly in the
11 lower stratosphere (Fig. 2). When the SF₆-corrected model ages were used, the age-based CO₂
12 reconstruction successfully reproduced the observed rate of decrease for CO₂ with increasing
13 altitude in the stratosphere within a deviation of about 1.3 ppm (root mean square). In this
14 study, monthly averaged ACTM profiles were used after interpolating to the site location.

15 When the top measurement height was below the tropopause, the concentration measured at
16 the highest altitude was assumed to be maintained up to the tropopause. The local tropopause
17 height was obtained from the U.S. National Centers for Environmental Prediction (NCEP)
18 Global Forecast System (GFS), a global spectral numerical model based on primitive
19 dynamical equations that includes a suite of parameterizations for atmospheric physics (Sela,
20 1980; Kalnay et al., 1990). The model is under constant development and evaluation (e.g.,
21 Yang et al., 2006).

22 To extrapolate profiles to the surface, tower data obtained at the Meteorological Research
23 Institute (Tsukuba, 36.1°N, 140.1°E), the LEF, WBI, and WGC towers were used for aircraft
24 measurements obtained over Narita airport (Japan, NRT), Park Falls (Wisconsin, LEF), West
25 Branch (Iowa, WBI) and Walnut Grove (California, WGC), respectively (Inoue and Matsueda,

1996, Andrews et al., 2011). Tower data for NOAA sites were acquired from the NOAA web site (GMD Data Archive).

The concentration at the lowermost observation above the planetary boundary layer (PBL) was assumed to hold from that point to the top of the PBL. When there were observed data within the PBL, the concentration at the highest observation height within the PBL was extended to the PBL top, and that at the lowest observation height was extended to ground level. When there were no observation data within the PBL, the concentration of the lowermost observation above the PBL was assumed to hold to ground level. Local PBL heights for each site were obtained from NCEP GFS.

Figure 3 shows a schematic example of a profile constructed with these assumptions. Discontinuities between the observed profiles and ACTM stratospheric profiles were at most a few ppm (mean ~ 1 ppm, standard deviation ~ 1 ppm). No correction was applied to resolve this discontinuity, but it is considered to be a source of uncertainty in the assumed profile, as discussed in Sect. 4.

The profiles of dry air number density were calculated by using the data sets of monthly mean climatological temperature and pressure of the Committee on Space Research (COSPAR) International Reference Atmosphere (CIRA)-86 (e.g., Fleming et al., 1988, 1990), which are given at 5° latitude intervals between 80°N and 80°S for altitudes of 0 to 120 km. Values at each observation site were obtained by linear interpolation of CIRA-86 data between two 5° grid points. Monthly mean values were adopted without interpolation in time.

XCO_2 was calculated by numerical integration of CO_2 dry mole fractions weighted by the dry air density within 100-m layers from the ground up to 85 km. It was assumed that the atmosphere was well mixed within each layer. Column abundance above 85 km was roughly estimated to be less than 0.01%, which is small enough to be neglected in this study. If the

CO₂ mixing ratio (mole CO₂/mole air) and dry air number density in the i -th layer are $n(i)$ and $N(i)$, respectively, XCO₂ can be represented as

$$XCO_2 = \sum_{surface}^{85km} n(i) \times N(i) / N, \quad (1)$$

where N is the total column abundance of dry air; $N(i)$ is calculated by logarithmic interpolation of the vertical profile of CIRA-86 data with a vertical resolution of 2 km; and $n(i)$ is calculated by linear interpolation between two neighboring observed or constructed data points. Araki et al. (2010) used only clear sky data for their analysis, whereas no screening by the weather conditions was done in this study.

The uncertainty of the XCO₂ calculation caused by the profile assumptions was estimated for each flight. In this study, the focus is on the upper limit of the uncertainty, because that value is most important for the validation of satellite observations. Because XCO₂ is the weighted mean of CO₂ concentrations calculated by the dry air abundance in each layer, its uncertainty was determined by the assumed uncertainties of the partial XCO₂ values and their weights. In this study, the uncertainty was defined as the standard deviation. We did not take into account the uncertainty of the dry air number density $N(i)$ (i.e., no variance) in this study because the XCO₂ values calculated by using the CIRA-86 number densities agreed with rawinsonde values obtained over Tsukuba within 0.1 ppm (Araki et al., 2010). The profiles were divided into four domains, within each of which the uncertainty of the data was treated as uniform: domain I, inside the PBL; domain II, region above the PBL with observed data; domain III, troposphere above the PBL without observed data; and domain IV, stratosphere without observed data. The uncertainty of total XCO₂ is represented as follows:

$$\text{Uncertainty} = \frac{\sqrt{\sum_j N(j)^2 \times \sigma(j)^2}}{N} (j = I, II, III, IV), \quad (2)$$

where $\sigma(j)$ and $N(j)$ are the assumed uncertainty of partial XCO_2 and the partial dry air number density in the j -th domain, respectively, and N is the total sum of $N(j)$. It is difficult to determine the $\sigma(j)$ for each site from variance of the observed data because the amount of data is not enough for some sites. Therefore, we assumed the maximal $\sigma(j)$ common for all sites based on analysis of the observed data, which will be discussed in Sect. 4. $\sigma(I)$ was assumed to be 15 ppm for flights with no data in the PBL or 2.89 ppm (corresponding to a uniform distribution within ± 5 ppm) for flights with data in the PBL. $\sigma(II)$ was assumed to be 0.4 ppm, and $\sigma(III)$ and $\sigma(IV)$ were assumed to be 1.73 ppm (corresponding to a uniform distribution within ± 3 ppm) (Table 2). The total uncertainty was determined from the height of the tropopause and the PBL, the uppermost and lowermost observation altitudes, the partial dry air abundances $N(j)$, and the uncertainties of partial XCO_2 $\sigma(j)$. The values of $\sigma(j)$ are critical for the estimation of total uncertainty, and their validity is discussed in Sect. 4.

4 Results and Discussion

Figure 4 shows the calculated XCO_2 values and their uncertainties derived from the profile assumptions between 2007 and 2009 at typical 7 sites, that is NRT, NGO, CGK, BNE (NOAA), RTA, SGP and SUR. Results for all the 53 sites are shown in the Supplementary materials (Fig. A-1, A-2 and A-3). As a visual guide, the following function was fitted to the XCO_2 data:

$$XCO_2(t) = a_1 + a_2 \times t + a_3 \times \cos(2\pi \frac{t - a_4}{365.25}) + a_5 \times \cos(4\pi \frac{t - a_6}{365.25}) \quad (3)$$

where a_1 is the intercept at the zero time point (1 January 2007) without sinusoidal variations, a_2 represents the yearly trend of XCO_2 , a_3 and a_5 are the amplitudes of sinusoidal variations with a period of one year and a half year, respectively, and a_4 and a_6 are the phases of each sinusoidal variation. Annual sinusoidal variations and their latitudinal dependence are clearly

seen. The amplitude of the seasonal cycle decreases from about 10 ppm at high latitudes in the Northern Hemisphere to 2 ppm or less in the tropics and the Southern Hemisphere. Compared with XCO_2 at NRT in 2007, calculated by Araki et al. (2010), the temporal behavior of XCO_2 is typically the same within our uncertainties.

The uncertainty estimation can be validated by comparing the partial XCO_2 value calculated from the observed profile with the fitted profile for each domain. For domain I (PBL), the data sets containing observed data in the PBL were chosen and the CO_2 concentrations at 5 km and 200 m were compared with the partial XCO_2 in the PBL. The concentration at 5 km corresponds to the partial XCO_2 assumed when a profile has no observed data in the PBL. The concentration at 200 m corresponds to the partial XCO_2 assumed when a profile has only one observed datum in the PBL. For this analysis, sites that had sufficient observations in the PBL to evaluate the “true” partial XCO_2 in the PBL were chosen. Therefore, sites with tower data were used for this analysis. The root mean square (RMS) of the deviation of the assumed partial XCO_2 from the observed partial XCO_2 was calculated. These comparisons show that the RMS in domain I was less than 3 ppm for flights with PBL data observations, and it was at most 15 ppm for flights without PBL data. These values agree with our assumptions about partial uncertainties.

For domain II (observation region above the PBL), the reported standard deviation of the measurements was typically 0.2 ppm. Here, we assumed that $\sigma(II)$ was 0.4 ppm, which corresponds to 2σ .

For domain III (troposphere without observations above the PBL), the data sets containing observed data from the top of the PBL to the tropopause were chosen to evaluate the “true” partial XCO_2 of the whole troposphere above the PBL and the CO_2 concentrations at 5 km were compared with the partial XCO_2 calculated from the observed profile. Here, the CO_2

1 concentration at 5 km was assumed to be the partial XCO_2 when only one observation was
2 available in the troposphere above the PBL. This analysis can determine the upper limit of
3 uncertainties in domain III because nearly all data sets include many observations in the
4 troposphere above the PBL. The comparison showed that the uncertainty in domain III was at
5 most 1.5 ppm, so the assumption of 1.73 ppm (the standard deviation corresponding to a
6 uniform distribution within ± 3 ppm) is a good approximation, though slightly high.

7 For domain IV (stratosphere without observation data), it is difficult to obtain an “observed”
8 partial XCO_2 , so the difference between the uppermost observed data in the stratosphere and
9 the nearest corrected age of air estimate from the ACTM was used. The standard deviations of
10 the errors were from 1.5 to 2.0 ppm, so the assumption of 1.73 ppm appears reasonable.

11 The total uncertainties calculated (Eq. 2) from all of the profile assumptions were at most 2
12 ppm and typically between 0.5 and 1.0 ppm. The uncertainty values strongly depended on
13 whether observations from the PBL were available. They were large at CONTRAIL sites
14 where the lowermost observation altitudes were relatively high, often above the top of the
15 PBL. At NRT, the use of Tsukuba tower data reduced the uncertainty to less than 1 ppm.
16 When tower data were not available, the uncertainty at NRT was large. The uncertainties at
17 NOAA and NIES sites were basically uniform with values less than 1 ppm. At the NOAA
18 sites with the largest uncertainties (AAO, LEF, SGP, and WGC), the uncertainties were
19 nearly 1 ppm. At these sites, the uppermost observation altitude was typically ~ 4000 m, which
20 is lower than at the other sites and caused the uncertainties to be larger. At PFA, the
21 uncertainties were also large, in this case because the height of the lowermost observation was
22 often above the top of the PBL. It is difficult to detect any seasonal behavior of the
23 uncertainties at CONTRAIL sites, where the uppermost observation altitude was relatively
24 high. For reference, frequency distributions of the estimated uncertainties at NRT, NGO,
25 AAO, BNE (NOAA), and SUR are shown in Fig. 5.

Araki et al. (2010) estimated the uncertainties derived from the CIRA-86 dry air number density data and the NCEP tropopause height data by comparing their results obtained with NCEP and CIRA-86 data with those obtained by using rawinsonde measurement data instead. They estimated the uncertainty from the CIRA-86 data to be 0.08 ppm, which is relatively insignificant compared with our estimated total uncertainties. They did not report the uncertainties from the NCEP tropopause heights, but they estimated the uncertainties from both the NCEP tropopause height and their assumptions about profiles near the surface to be 0.92 ppm (Araki et al., 2010). Therefore, the uncertainties from the NCEP tropopause height were also small because the uncertainties from the profiles near the surface were dominant and can be treated as part of the uncertainties derived from the profile assumptions, as described above. In addition, we investigated the impact of the PBL heights on the XCO₂ calculation. The differences between “XCO₂ where PBL heights are true values (PBL_{true} XCO₂)” and “XCO₂ where they are assumed to be 1500 m (PBL₁₅₀₀ XCO₂) or 200 m (PBL₂₀₀ XCO₂)” are estimated at NRT, AMS, SYD, and HNL sites. At AMS, the differences between PBL_{true} XCO₂ and PBL₁₅₀₀ XCO₂ (PBL_{true} XCO₂ minus PBL₁₅₀₀ XCO₂) are less than ±0.21 ppm at most, and average of the differences and one standard deviation are 0.00 ± 0.03 ppm. On the other hand, the differences between PBL_{true} XCO₂ and PBL₂₀₀ XCO₂ (PBL_{true} XCO₂ minus PBL₂₀₀ XCO₂) at AMS are less than ±0.20 ppm at most and 0.00 ± 0.03 ppm on average. Also we found that the impact of PBL heights on the aircraft-based XCO₂ calculation is not large at other sites.

5 Conclusions

XCO₂ at 53 sites in the world was calculated from aircraft measurement data obtained by CONTRAIL, NOAA, and NIES between 2007 and 2009 along with tower data obtained at the

1 surface and the ACTM simulated age of air to estimate profiles in the stratosphere. The
2 amplitudes of seasonal cycles decreased from north to south. The estimated upper limits of
3 the uncertainties of XCO₂ were typically less than 1 ppm, suggesting that this data set is
4 suitable for evaluation of XCO₂ estimates by satellites.

5 Recently, XCO₂ has been derived from data obtained by satellites, such as GOSAT (Yokota et
6 al., 2009), the Scanning Imaging Absorption Spectrometer for Atmospheric Chartography
7 (SCIAMACHY; Bovensmann et al., 1999) onboard ENVISAT, and the Atmospheric Infrared
8 Sounder (AIRS; Crevoisier et al., 2004) onboard NASA's Aqua platform. These satellite data
9 are considered useful for decreasing the flux estimation errors in global atmospheric transport
10 models and for investigating CO₂ sources and the carbon cycle in more detail. However, it is
11 necessary to validate these data for such scientific applications. The profile data of aircraft
12 measurements cannot be directly compared with the column-averaged data from satellites. In
13 this work, we therefore propose a method for converting the profile data from aircraft to
14 column-averaged data and for estimating the uncertainties of the calculated values. Our
15 analysis suggests that the uncertainties are small enough for the aircraft data to be used for
16 primary validation of satellite data. When comparing XCO₂ derived from the satellite
17 measurements such as GOSAT with the aircraft data, the column averaging kernels (CAKs)
18 of satellite measurements should be taken into account. Although much attention needs to be
19 paid to using this XCO₂ dataset since it is not calculated with consideration of CAKs, it is
20 very useful within the scientific community. Therefore, we would like to provide it on request.
21 Furthermore, it should be possible to extend the method to other species such as methane
22 using tracer-tracer correlation method or climatology of satellite data.

24 Acknowledgements

We acknowledge the many staff members of Japan Airlines, the JAL Foundation, and JAMCO Tokyo for supporting the CONTRAIL project. We also thank Takakiyo Nakazawa for providing the balloon-borne data. The NOAA/ESRL Tall Tower project relies heavily on partnerships with universities and other agencies. Individuals who have made significant contributions to the data set used in this study include Ankur Desai of the University of Wisconsin (LEF), Charles Stanier of the University of Iowa (WBI), and Marc Fischer of Lawrence Berkeley National Laboratory (WGC). This research was supported in part by the Environment Research and Technology Development Fund (A-1102) of the Ministry of the Environment, Japan.

References

- Andrews, A. E., Boering, K. A., Daube, B. C., Wofsy, S. C., Loewenstein, M., Jost, H., Podolske, J. R., Webster, C. R., Herman, R. L., Scott, D. C., Flesch, G. J., Moyer, E. J., Elkins, J. W., Dutton, G. S., Hurst, D. F., Moore, F. L., Ray, E. A., Romashkin, P. A., Strahan, S. E.: Mean ages of stratospheric air derived from in situ observations of CO₂, CH₄, and N₂O, *J. Geophys. Res.*, 106, 32295–32314, doi:10.1029/2001JD000465, 2001.
- Andrews, A. E., Kofler J., Bakwin P. S., Zhao C., Tans P.: Carbon dioxide and carbon monoxide dry air mole fractions from the NOAA ESRL tall tower network, 1992-2009, Version: 2011-08-31, Path: <ftp://ftp.cmdl.noaa.gov/ccg/towers/>, 2011.
- Araki, M., Morino, I., Machida, T., Sawa, Y., Matsueda, H., Ohyama, H., Yokota, T., and Uchino, O.: CO₂ column-averaged volume mixing ratio derived over Tsukuba from measurements by commercial airlines, *Atmos. Chem. Phys.*, 10, 7659–7667, doi:10.5194/acp-10-7659-2010, 2010.

1 Austin, J., and Li, F.: On the relationship between the strength of the Brewer-Dobson
2 circulation and the age of stratospheric air, *Geophys. Res. Lett.*, 33, L17807,
3 doi:10.1029/2006GL026867, 2006.

4 Bovensmann, H., Burrows, J. P., Buchwitz, M., Frerick, J., Noël, S., Rozanov, V. V., Chance,
5 K. V., Goede, A. P. H.: SCIAMACHY: Mission Objectives and Measurement Modes, *J.*
6 *Atmos. Sci.*, 56, 127-150, 1999.

7 COSPAR (Committee on Space Research): The COSPAR International Reference
8 Atmosphere (CIRA-86), British Atmospheric Data Center,
9 http://badc.nerc.ac.uk/view/badc.nerc.ac.uk__ATOM__dataent_CIRA.

10 Crevoisier, C., Heilliette, S., Chédin, A., Serrar, S., Armante, R., and Scott, N. A.:
11 Midtropospheric CO₂ concentration retrieval from AIRS observations in the tropics, *Geophys.*
12 *Res. Lett.*, 31, L17106, doi:10.1029/2004GL020141, 2004.

13 Engel, A., Möbius, T., Bönisch, H., Schmidt, U., Heinz, R., Levin, I., Atlas, E., Aoki, S.,
14 Nakazawa, T., Sugawara, S., Moore, F., Hurst, D., Elkins, J., Schauffler, S., Andrews, A.,
15 Boering, K.: Age of stratospheric air unchanged within uncertainties over the past 30 years,
16 *Nature Geoscience*, 2, 28-31, doi:10.1038/ngeo388, 2009.

17 Fleming, E. L., Chandra, S., Shoeberl, M. R., and Barnett, J. J., Monthly mean global
18 climatology of temperature, wind, geopotential height and pressure for 0-120 km, National
19 Aeronautics and Space Administration, Technical Memorandum 100697, Washington, D.C.,
20 1988.

21 Fleming, E. L., Chandra, S., Barnett, J. J., and Corney, M.: Zonal mean temperature, pressure,
22 zonal wind and geopotential height as functions of latitude, *Adv. Space Res.*, 10(12), 11-59,
23 doi:10.1016/0273-1177(90)90386-E, 1990.

1 GMD Data Archive: Global Monitoring Division, Earth System Research Laboratory, NOAA,
2 <http://www.esrl.noaa.gov/gmd/dv/ftpdata.html>.

3 Harnisch, J., Borchers, R., Fabian, P., and Maiss, M.: Tropospheric trends for CF₄ and C₂F₆
4 since 1982 derived from SF₆ dated stratospheric air, *Geophys. Res. Lett.*, 23, 1099-1102,
5 doi:10.1029/96GL01198, 1996.

6 Inoue, H. Y. and Matsueda, H.: Variations in atmospheric CO₂ at the Meteorological
7 Research Institute, Tsukuba, Japan, *J. Atmos. Chem.*, 23, 137-161, 1996.

8 Ishidoya, S., Sugawara, S., Morimoto, S., Aoki S., and Nakazawa T.: Gravitational separation
9 of major atmospheric components of nitrogen and oxygen in the stratosphere, *Geophys. Res.*
10 *Lett.*, 35, L03811, doi:10.1029/2007GL030456, 2008.

11 Kalnay, E., Kanamitsu, M., and Baker, W. E.: Global numerical weather prediction at the
12 National Meteorological Center, *Bull. Amer. Meteor. Soc.*, 71, 1410-1428, 1990.

13 Kuze, A., Suto, H., Nakajima, M., and Hamazaki, T.: Thermal and near infrared sensor for
14 carbon observation Fourier-transform spectrometer on the Greenhouse Gases Observing
15 Satellite for greenhouse gases monitoring, *Applied Optics*, 48, 6716-6733
16 doi:10.1364/AO.48.006716, 2009.

17 Machida, T., Nakazawa, T., Ishidoya, S., Maksyutov, S., Tohjima, Y., Takahashi, Y., Watai,
18 T., Vinnichenko, N., Panchenko, M., Arshinov, M., Fedoseev, N., and Inoue, G.: Temporal
19 and spatial variations of atmospheric CO₂ mixing ratio over Siberia, *Proceedings of The Sixth*
20 *International CO₂ Conference*, Sendai, Japan, 1-5 October, 2001.

21 Machida, T., Matsueda, H., Sawa, Y., Nakagawa, Y., Hirotsu, K., Kondo, N., Goto, K.,
22 Nakazawa, T., Ishikawa, K., and Ogawa, T.: Worldwide Measurements of Atmospheric CO₂
23 and Other Trace Gas Species Using Commercial Airlines, *J. Atmos. Oceanic. Technol.*, 25,
24 1744, doi: 10.1175/2008JTECHA1082.1, 2008.

1 Machida, T., Tohjima, Y., Katsumata, K., and Mukai, H.: A new CO₂ calibration scale based
2 on gravimetric one-step dilution cylinders in National Institute for Environmental Studies -
3 NIES 09 CO₂ scale, GAW Report, 194, 114-119, 15th WMO/IAEA Meeting of Experts on
4 Carbon Dioxide, Other Greenhouse Gases and Related Tracers Measurement Techniques,
5 WMO/TD No. 1553, 2011.

6 Miller, C. E., Crisp, D., DeCola, P. L., Olsen, S. C., Randerson, J. T., Michalak, A. M.,
7 Alkhaled, A., Rayner, P., Jacob, D. J., Suntharalingam, P., Jones, D. B. A., Denning, A. S.,
8 Nicholls, M. E., Doney, S. C., Pawson, S., Bösch, H., Connor, B. J., Fung, I. Y., O'Brien, D.,
9 Salawitch, R. J., Sander, S. P., Sen, B., Tans, P., Toon, G. C., Wennberg, P. O., Wofsy, S. C.,
10 Yung, Y. L., and Law, R. M.: Precision requirements for space-based XCO₂ data, *J. Geophys.*
11 *Res.*, 112, D10314, doi:10.1029/2006JD007659, 2007.

12 Morino, I., Uchino, O., Inoue, M., Yoshida, Y., Yokota, T., Wennberg, P. O., Toon, G. C.,
13 Wunch, D., Roehl, C. M., Notholt, J., Warneke, T., Messerschmidt, J., Griffith, D. W. T.,
14 Deutscher, N. M., Sherlock, V., Connor, B., Robinson, J., Sussmann, R., and Rettinger, M.:
15 Preliminary validation of column-averaged volume mixing ratios of carbon dioxide and
16 methane retrieved from GOSAT short-wavelength infrared spectra, *Atmos. Meas. Tech.*, 4, 1-
17 16, doi:10.5194/amt-4-1-2011, 2011.

18 Nakazawa, T., Machida, T., Sugawara, S., Murayama, S., Morimoto, S., Hashida, G., Honda,
19 H., and Itoh, T.: Measurements of the stratospheric carbon dioxide concentration over Japan
20 using a balloon-borne cryogenic sampler, *Geophys. Res. Lett.*, 22, 1229-1232,
21 doi:10.1029/95GL01188 , 1995.

22 NCEP: NOAA/National Weather Service, National Center for Environmental Prediction,
23 NCEP Internet Services Team, <http://www.ncep.noaa.gov/>.

1 NOAA/ESRL Carbon Cycle Greenhouse Gases Aircraft Program, Web:
2 <http://www.esrl.noaa.gov/gmd/ccgg/aircraft/index.html>.

3 Patra, P. K., Lal, S., Subbaraya, B. H., Jackman, C. H., and Rajaratnam, P.: Observed vertical
4 profile of sulphur hexafluoride (SF₆) and its atmospheric applications, *J. Geophys. Res.*, 102,
5 8855-8859, 1997.

6 Patra, P. K., Maksyutov, S., Sasano, Y., Nakajima, H., Inoue, G., and Nakazawa, T.: An
7 evaluation of CO₂ observations with Solar Occultation FTS for Inclined-Orbit Satellite sensor
8 for surface source inversion, *J. Geophys. Res.*, 108, D24, 4759, doi:10.1029/2003JD003661,
9 2003.

10 Patra, P. K., Takigawa, M., Dutton, G. S., Uhse, K., Ishijima, K., Lintner, B. R., Miyazaki, K.,
11 and Elkins, J. W.: Transport mechanisms for synoptic, seasonal and interannual SF₆ variations
12 and "age" of air in troposphere, *Atmos. Chem. Phys.*, 9, 1209-1225, 2009.

13 Rayner, P. J., Law, R. M., O'Brien, D. M., Butler, T. M., and Dilley, A. C.: Global
14 observations of the carbon budget 3. Initial assessment of the impact of satellite orbit, scan
15 geometry, and cloud on measuring CO₂ from space, *J. Geophys. Res.*, 107, D21,
16 doi:10.1029/2001JD000618, 2002.

17 Schneising, O., Bergamaschi, P., Bovensmann, H., Buchwitz, M., Burrows, J. P., Deutscher,
18 N. M., Griffith, D. W. T., Heymann, J., Macatangay, R., Messerschmidt, J., Notholt, J.,
19 Rettinger, M., Reuter, M., Sussmann, R., Velasco, V. A., Warneke, T., Wennberg, P. O., and
20 Wunch, D.: Atmospheric greenhouse gases retrieved from SCIAMACHY: comparison to
21 ground-based FTS measurements and model results, *Atmos. Chem. Phys.*, 12, 1527-1540,
22 doi:10.5194/acp-12-1527-2012, 2012.

23 Sela, J.: Spectral modeling at the National Meteorological Center, *Mon. Wea. Rev.*, 108,
24 1279-1292, 1980.

1 Tans, P. P., Bakwin, P. S., Conway, T. J., Dissly, R. W., Dlugokencky, E. J., Geller, L. S.,
2 Guenther, D. W., Hurst, D. F., Kitzis, D. R., Lang, P. M., Masarie, K. A., Miller, J. B.,
3 Novelli, P. C., Prostko-Bell, C., Ramonet, M., Thoning, K. W., Troler, M., Waterman, L.S.,
4 Zhang, N., and Zhao, C.: Carbon Cycle (Group Report), Climate Monitoring and Diagnostics
5 Laboratory, No. 23, Summary Report 1994-1995, Hoffman, D. J., J. T. Peterson and R. M.
6 Rosson, eds, US Department of Commerce, Boulder, Colorado, 1996.

7 WDCGG: WMO Global Atmosphere Watch, World Data Centre for Greenhouse Gases,
8 <http://ds.data.jma.go.jp/gmd/wdcgg/>.

9 WMO: WMO Greenhouse Gas Bulletin, No. 3, World Meteorological Organization, 2006,
10 <http://www.wmo.int/pages/prog/arep/gaw/ghg/GHGbulletin.html>.

11 Wunch, D., Toon, G. C., Wennberg, P. O., Wofsy, S. C., Stephens, B. B., Fischer, M. L.,
12 Uchino, O., Abshire, J. B., Bernath, P., Biraud, S. C., Blavier, J. -F. L., Boone, C., Bowman,
13 K. P., Browell, E. V., Campos, T., Connor, B. J., Daube, B. C., Deutscher, N. M., Diao, M.,
14 Elkins, J. W., Gerbig, C., Gottlieb, E., Griffith, D. W. T., Hurst, D. F., Jimenez, R., Keppel-
15 Aleks, G., Kort, E. A., Macatangay, R., Machida, T., Matsueda, H., Moore, F., Morino, I.,
16 Park, S., Robinson, J., Roehl, C. M., Sawa, Y., Sherlock, V., Sweeney, C., Tanaka, T., and
17 Zondlo, M. A.: Calibration of the Total Carbon Column Observing Network using aircraft
18 profile data, *Atmos. Meas. Tech.*, 3, 1351-1362, doi:10.5194/amt-3-1351-2010, 2010.

19 Wunch, D., Toon, G. C., Blavier, J.-F. L., Washenfelter, R. A., Notholt, J., Connor, B. J.,
20 Griffith, D. W. T., Sherlock, V., and Wennberg, P. O.: The Total Carbon Column Observing
21 Network, *Philos. T. Roy. Soc. A*, 369, 2087-2112, doi:10.1098/rsta.2010.0240, 2011a.

22 Wunch, D., Wennberg, P. O., Toon, G. C., Connor, B. J., Fisher, B., Osterman, G. B.,
23 Frankenberg, C., Mandrake, L., O'Dell, C., Ahonen, P., Biraud, S. C., Castano, R., Cressie, N.,
24 Crisp, D., Deutscher, N. M., Eldering, A., Fischer, M. L., Griffith, D. W. T., Gunson, M.,

1 Heikkinen, P., Keppel-Aleks, G., Kyrö, E., Lindenmaier, R., Macatangay, R., Mendonca, J.,
 2 Messerschmidt, J., Miller, C. E., Morino, I., Notholt, J., Oyafuso, F. A., Rettinger, M.,
 3 Robinson, J., Roehl, C. M., Salawitch, R. J., Sherlock, V., Strong, K., Sussmann, R., Tanaka,
 4 T., Thompson, D. R., Uchino, O., Warneke, T., and Wofsy, S. C.: A method for evaluating
 5 bias in global measurements of CO₂ total columns from space, *Atmos. Chem. Phys.*, 11,
 6 12317-12337, doi:10.5194/acp-11-12317-2011, 2011b.
 7 Yang, F., Pan, H.-L., Krueger, S. K., Moorthi, S., and Lord, S. J.: Evaluation of the NCEP
 8 Global Forecast System at the ARM SGP site, *Mon. Wea. Rev.*, 134, 3668-3690, 2006.
 9 Yokota, T., Yoshida, Y., Eguchi, N., Ota, Y., Tanaka, T., Watanabe, H., and Maksyutov, S.:
 10 Global Concentrations of CO₂ and CH₄ Retrieved from GOSAT: First Preliminary Results,
 11 *SOLA*, 5, 160-163, doi:10.2151/sola.2009-041, 2009.
 12 Yoshida, Y., Ota, Y., Eguchi, N., Kikuchi, N., Nobuta, K., Tran, H., Morino, I., and Yokota,
 13 T.: Retrieval algorithm for CO₂ and CH₄ column abundances from short-wavelength infrared
 14 spectral observations by the Greenhouse gases observing satellite, *Atmos. Meas. Tech.*, 4,
 15 717-734, doi:10.5194/amt-4-717-2011, 2011.
 16 Zhu, X., Yee, J. -H., and Strobel, D. F.: Middle atmosphere age of air in a globally balanced
 17 two-dimensional model, *J. Geophys. Res.*, 105, 15201-15212, 2000.

18

Table 1. Locations of the sites where aircraft measurements were made.

(a) CONTRAIL

CODE	Latitude (°N)	Longitude (°E)	
AMS	52.3	4.8	Schiphol Airport, the Netherlands
LHR	51.5	−0.5	Heathrow Airport, UK
YVR	49.2	−123.2	Vancouver International Airport, Canada
CDG	49.0	2.5	Charles de Gaulle International Airport, France
MLP	45.6	8.7	Milan Malpensa International Airport, Italy
CTS	42.8	141.7	New Chitose Airport, Japan
FCO	41.8	12.3	Fiumicino Airport, Italy
ICN	37.5	126.5	Incheon International Airport, South Korea
NRT	35.8	140.4	Narita International Airport, Japan
HND	35.6	139.8	Tokyo International Airport, Japan
NGO	34.9	136.8	Chubu Centrair International Airport, Japan
ITM	34.8	135.4	Osaka International Airport, Japan
HIJ	34.4	132.9	Hiroshima Airport, Japan
KIX	34.4	135.2	Kansai International Airport, Japan
FUK	33.6	130.5	Fukuoka Airport, Japan
DEL	28.6	77.1	Indira Gandhi International Airport, India
OKA	26.2	127.6	Naha Airport, Japan
TPE	25.1	121.2	Taiwan Taoyuan International Airport, Taiwan
HNL	21.3	−157.9	Honolulu International Airport, USA
MEX	19.4	−99.1	Mexico City International Airport, Mexico
MNL	14.5	121.0	Ninoy Aquino International Airport, Philippines
BKK	13.7	100.7	Suvarnabhumi International Airport, Thailand
GUM	13.5	144.8	Guam International Airport, USA
SIN	1.4	104.0	Singapore Changi International Airport, Singapore
CGK	−6.1	106.7	Jakarta International Soekarno-Hatta Airport, Indonesia
DPS	−8.7	115.2	Ngurah Rai Airport, Indonesia
BNE	−27.4	153.1	Brisbane Airport, Australia
SYD	−33.9	151.2	Kingsford Smith Airport, Australia

(b) NOAA

CODE	Latitude (°N)	Longitude (°E)	
AAO	40.1	−88.6	Airborne Aerosol Observing, Illinois
BNE	40.8	−97.2	Beaver Crossing, Nebraska
BRM	54.3	−105.0	Berms, Saskatchewan
CAR	40.4	−104.3	Briggsdale, Colorado
CMA	38.8	−74.3	Cape May, New Jersey

DND	48.4	−97.8	Dahlen, North Dakota
ESP	49.6	−126.4	Estevan Point, British Columbia
HAA	21.2	−159.0	Molokai Island, Hawaii
HFM	42.5	−72.2	Harvard Forest, Massachusetts
HIL	40.1	−87.9	Homer, Illinois
LEF	45.9	−90.3	Park Falls, Wisconsin
NHA	43.0	−70.6	Worcester, Massachusetts
PFA	65.1	−147.3	Poker Flat, Alaska
RTA	−21.3	−159.8	Rarotonga, Cook Islands
SCA	32.8	−79.6	Charleston, South Carolina
SGP	36.8	−97.5	Southern Great Plains, Oklahoma
TGC	27.7	−96.9	Sinton, Texas
THD	41.1	−124.2	Trinidad Head, California
VAA	32.9	−79.4	Cartersville, Georgia
WBI	41.7	−91.4	West Branch, Iowa
WGC	38.3	−121.5	Walnut Grove, California

(c) NIES

CODE	Latitude (°N)	Longitude (°E)	
SGM	35.1	139.3	Sagami Bay, Japan
YAK	62	130	Yakutsk, Russia
NOV	55	83	Novosibirsk, Russia
SUR	61	73	Surgut, Russia

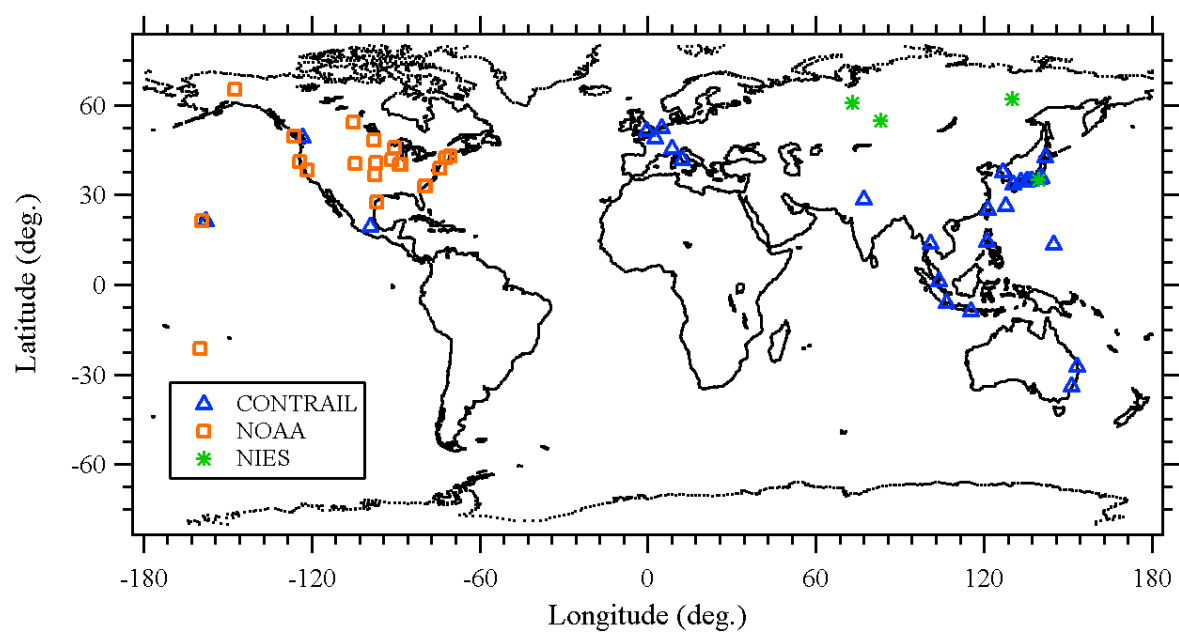
1

2 Table 2. The assumed standard deviations of partial XCO₂ in each domain.

Domain	Standard deviation (ppm)
I (No observed data in PBL)	15
I (With observed data in PBL)	2.89
II	0.4
III	1.73
IV	1.73

3

1



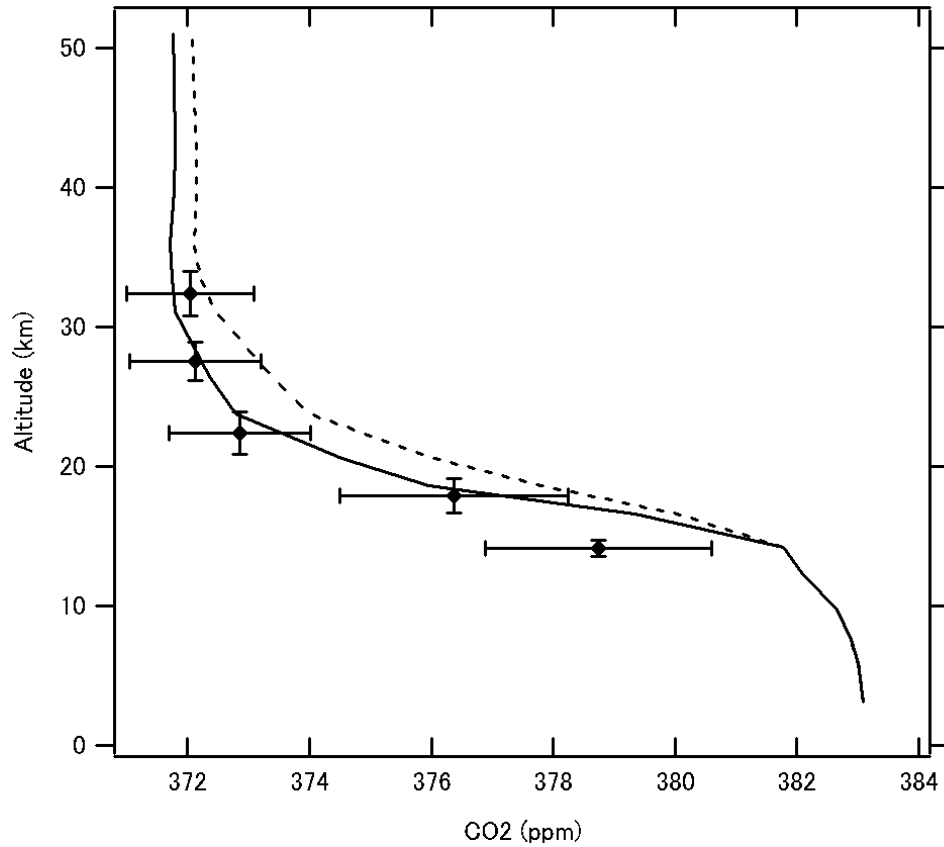
2

3

4 Figure 1. Observation sites used in this study. Open triangles, open squares, and asterisks
5 indicate CONTRAIL, NOAA, and NIES sites, respectively.

6

1



2

3 Figure 2. Calculated CO₂ profile at 40.5°N latitude from the modeled “age of air” (lines) and
 4 the observed profile (symbols) at Sanriku, Japan (39.2°N) in January 2007. The dashed line
 5 shows the ACTM modeled profile uncorrected by the observed SF₆ age of air, and the solid
 6 line shows the profile after normalization. Error bars of the observed data show the standard
 7 deviations of the mean.

8

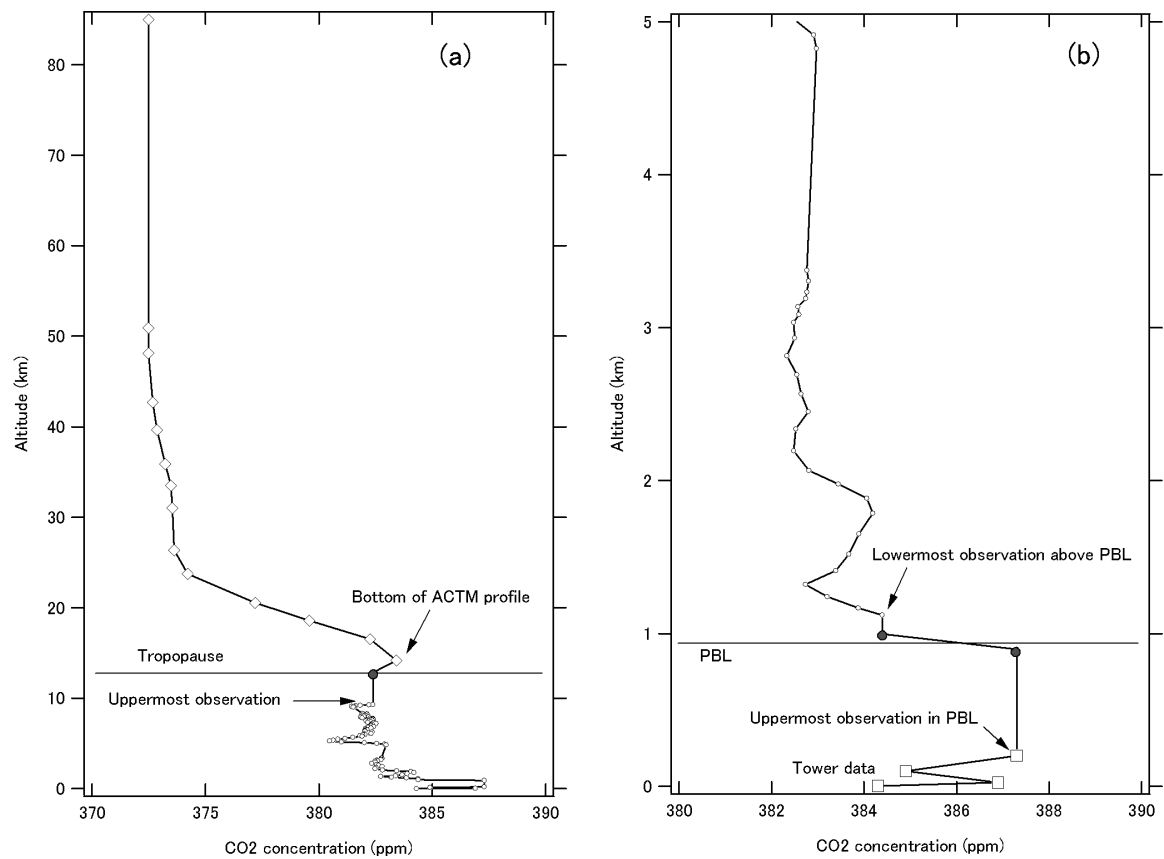
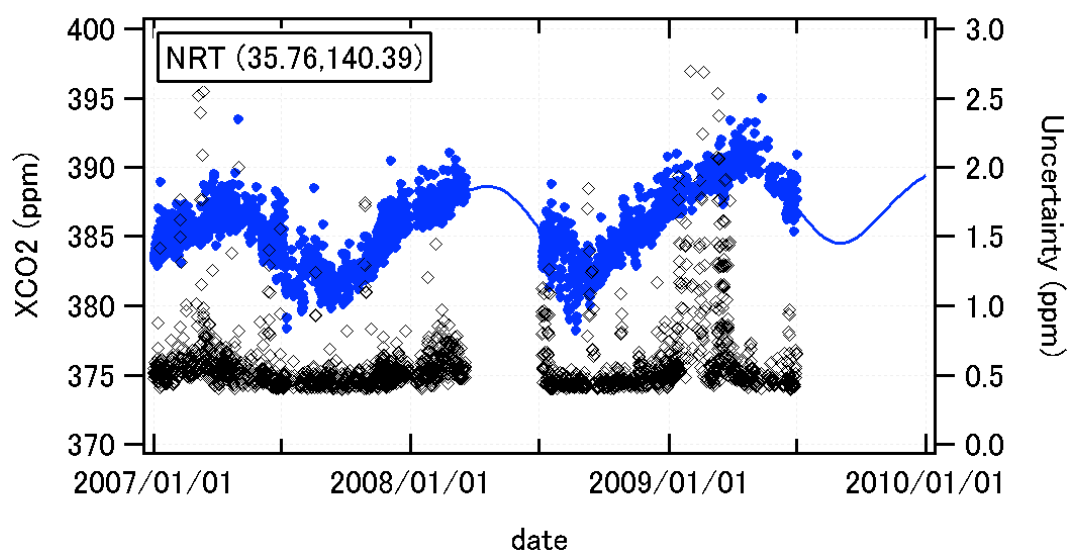


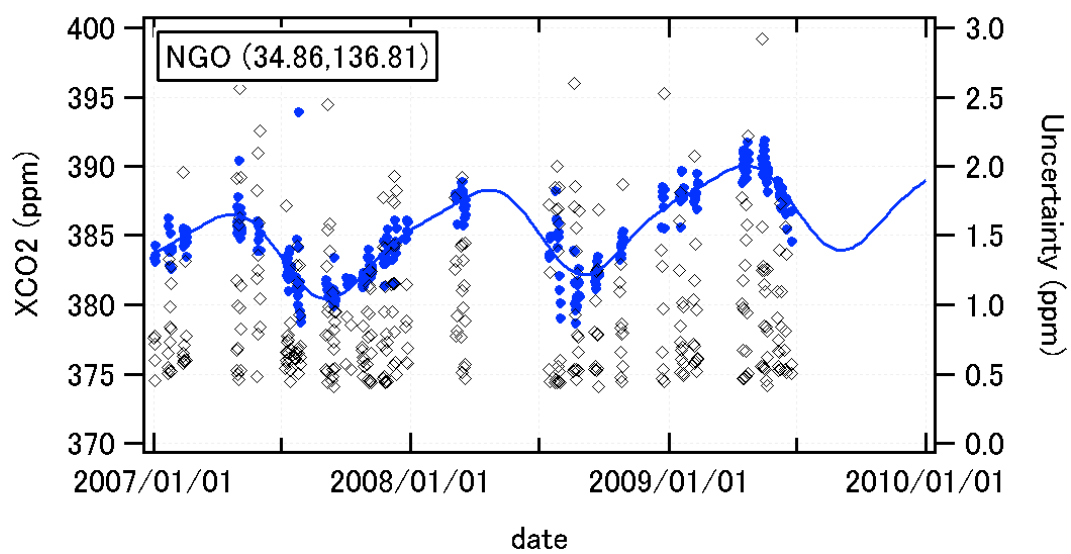
Figure 3. Schematic example of a vertical CO₂ profile: (a) the profile from the ground to 85 km; (b) an expanded view of the profile between the ground and 5 km. Open circles, squares, and diamonds show data observed by aircraft, data observed by towers, and the ACTM profile, respectively. Closed circles show the assumed value at the tropopause and the top of the PBL.

1

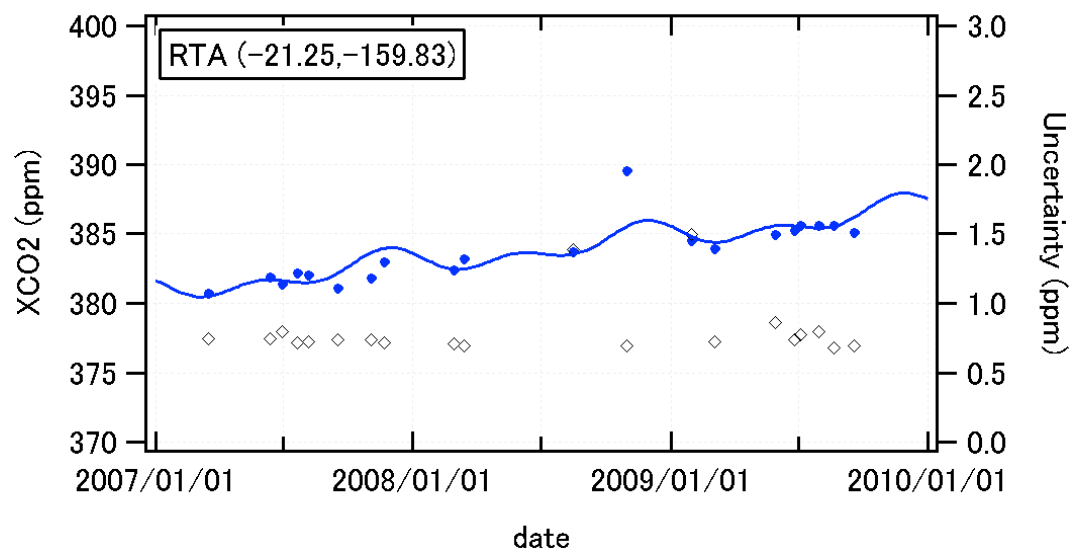
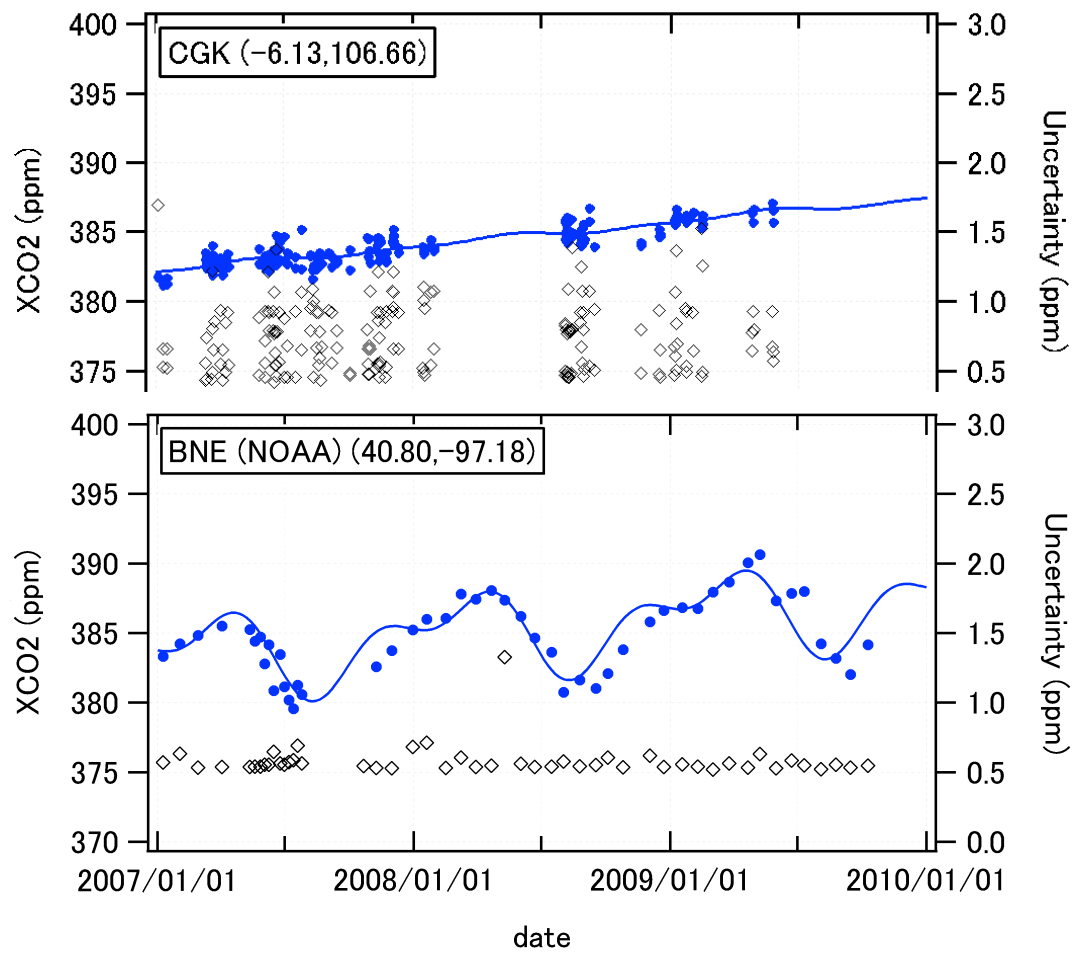
2 CONTRAIL



3



4



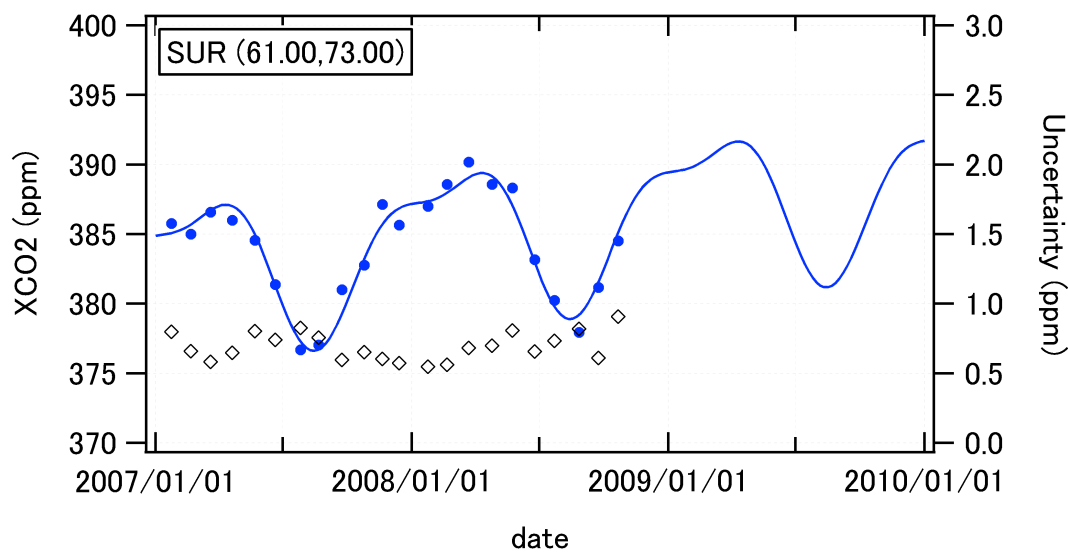
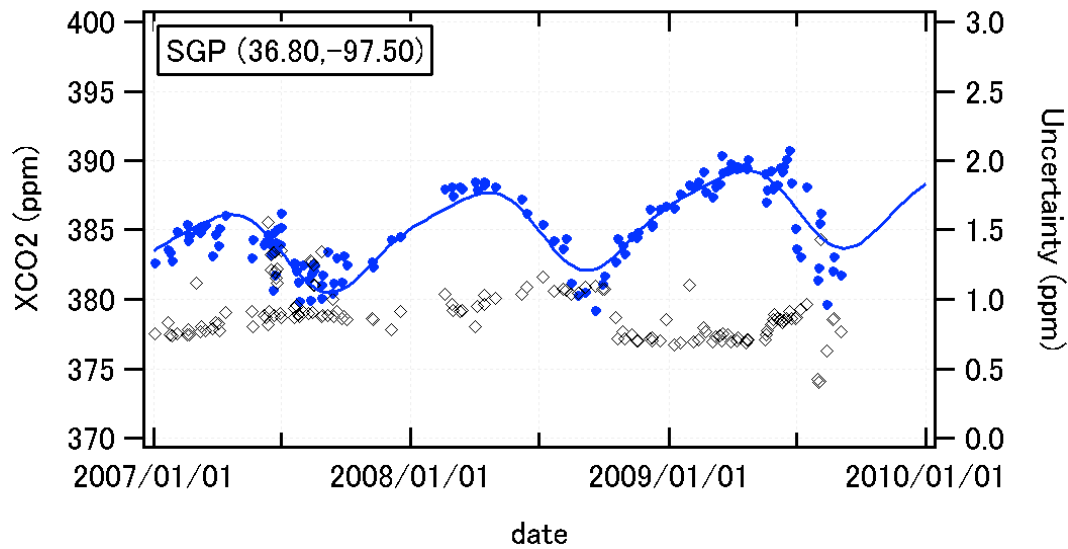
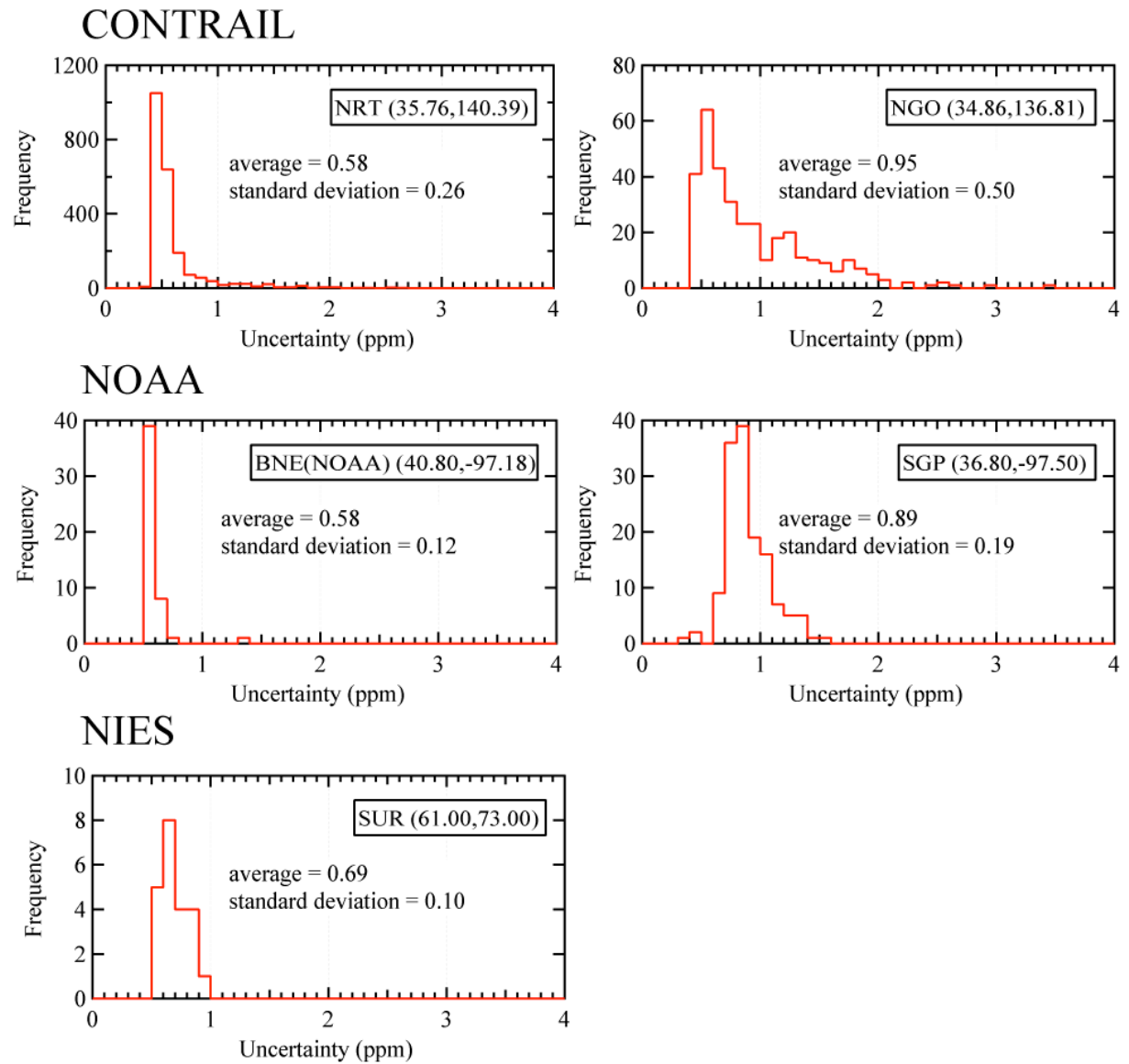


Figure 4. Calculated XCO_2 values and their estimated uncertainties at [NRT](#), [NGO](#), [BNE](#) ([NOAA](#)), [SGP](#) and [SUR](#). The site code (Table 1) and its latitude and longitude are shown at the upper left corner of each panel. Blue filled circles show XCO_2 (left axis), and black open rhomboids show their uncertainties (right axis). Blue solid lines show curves fitted to the temporal behavior of XCO_2 as a visual guide (only for sites where the number of data was sufficient).



1

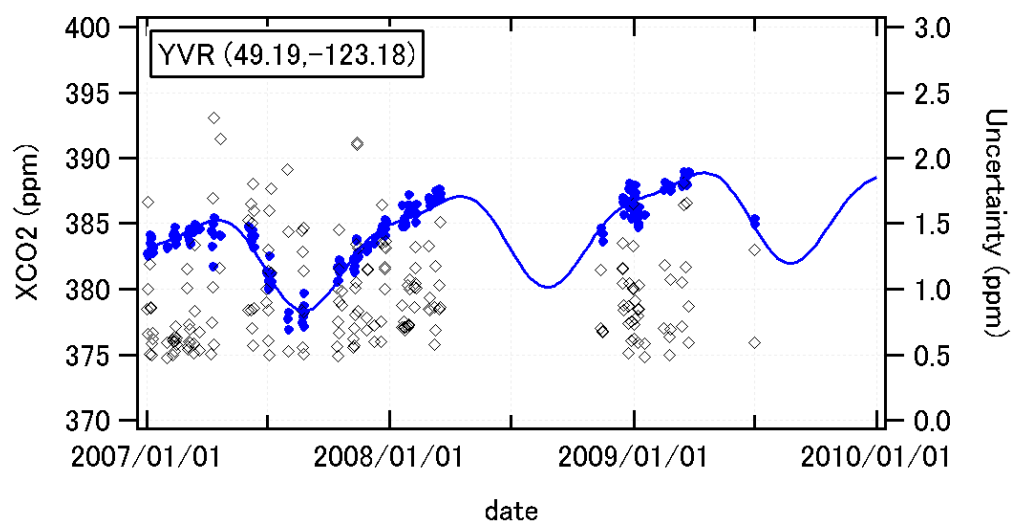
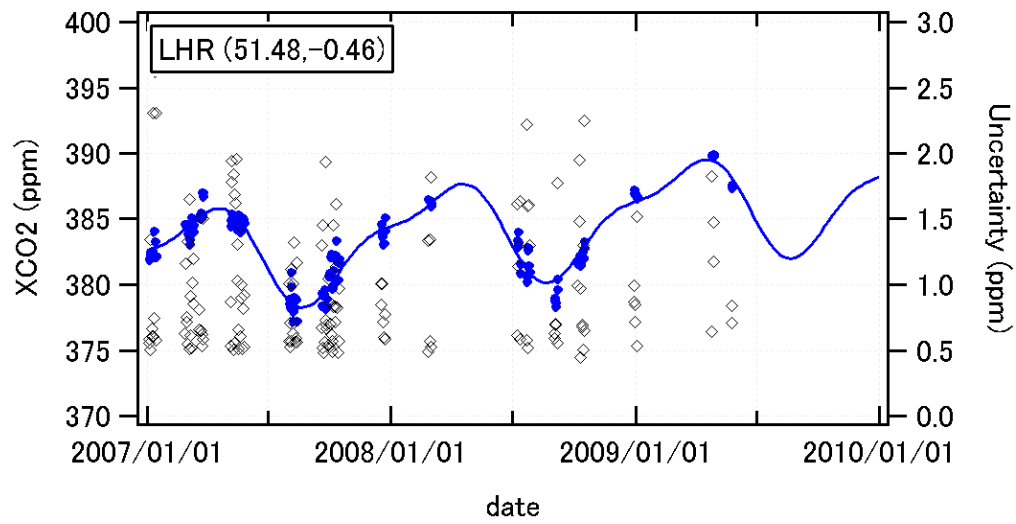
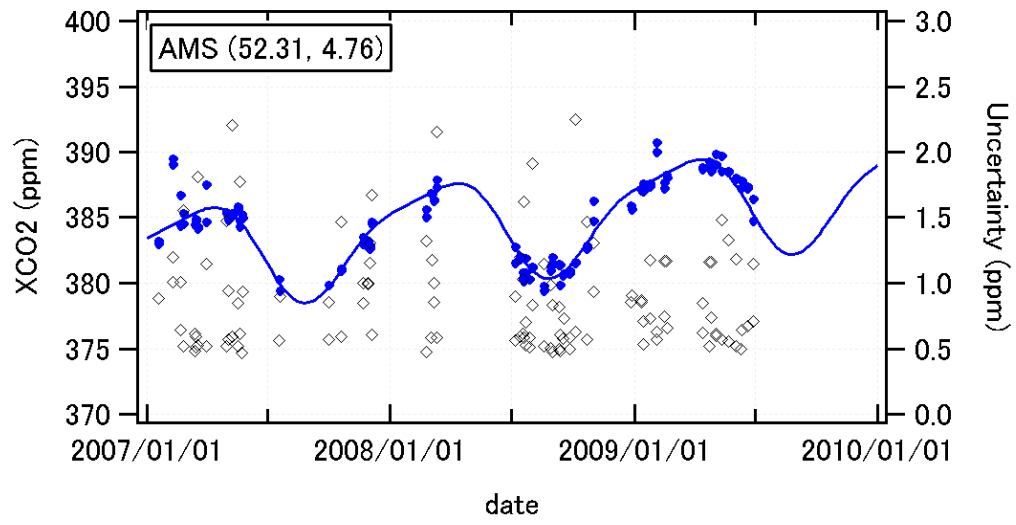
2 Figure 5. Frequency distributions of the estimated uncertainties at five sites. The size of each
 3 frequency class is 0.2 ppm.

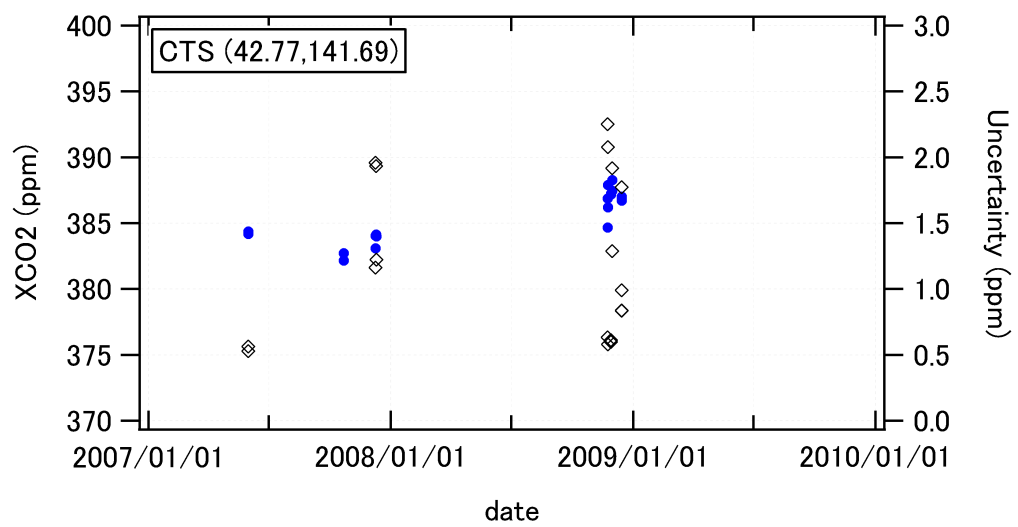
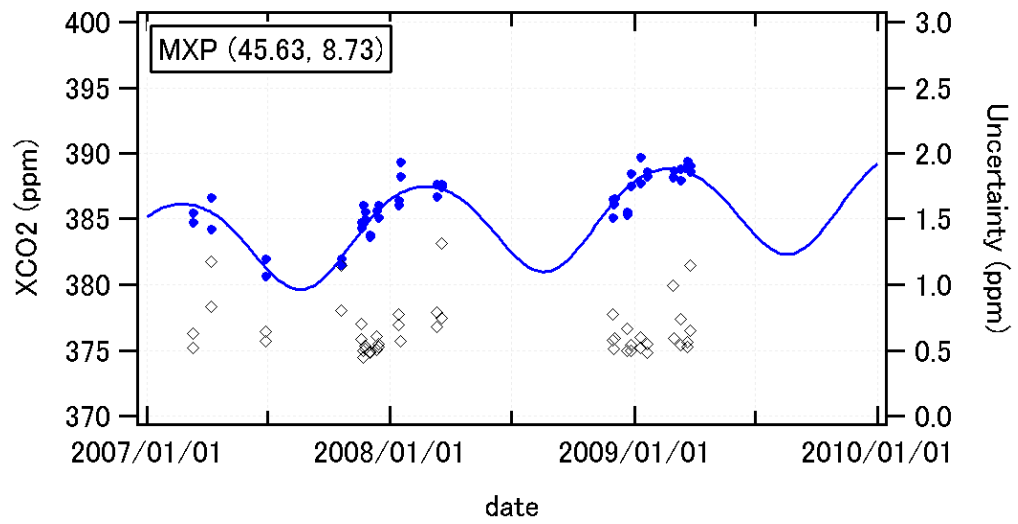
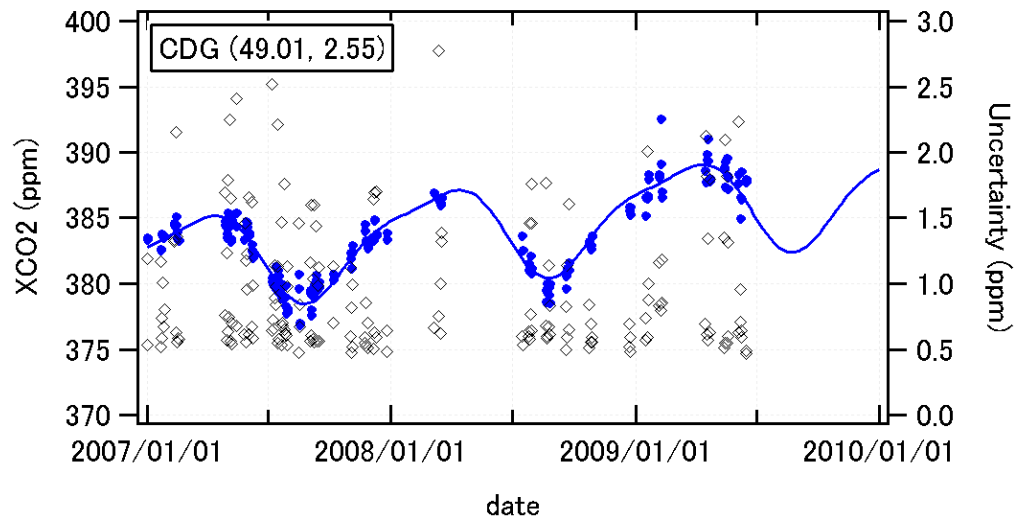
4

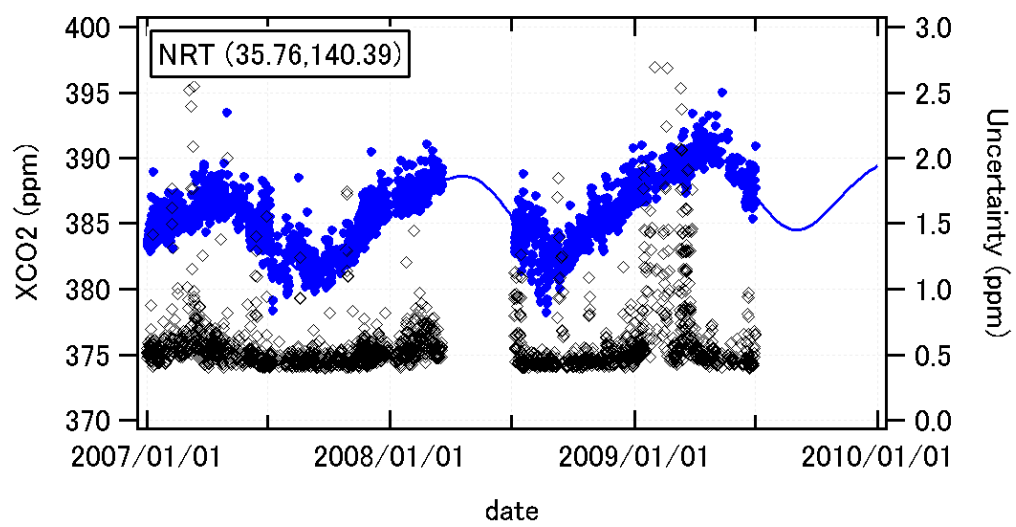
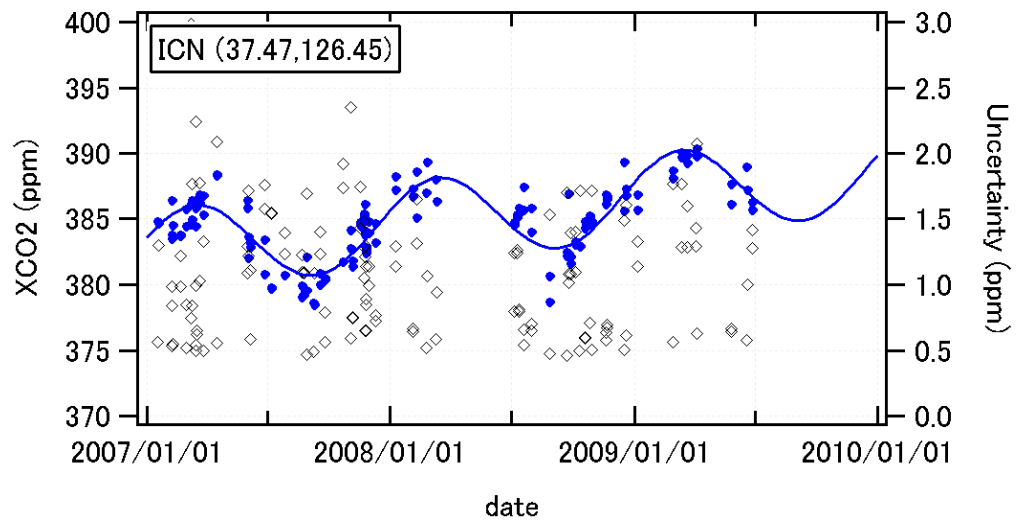
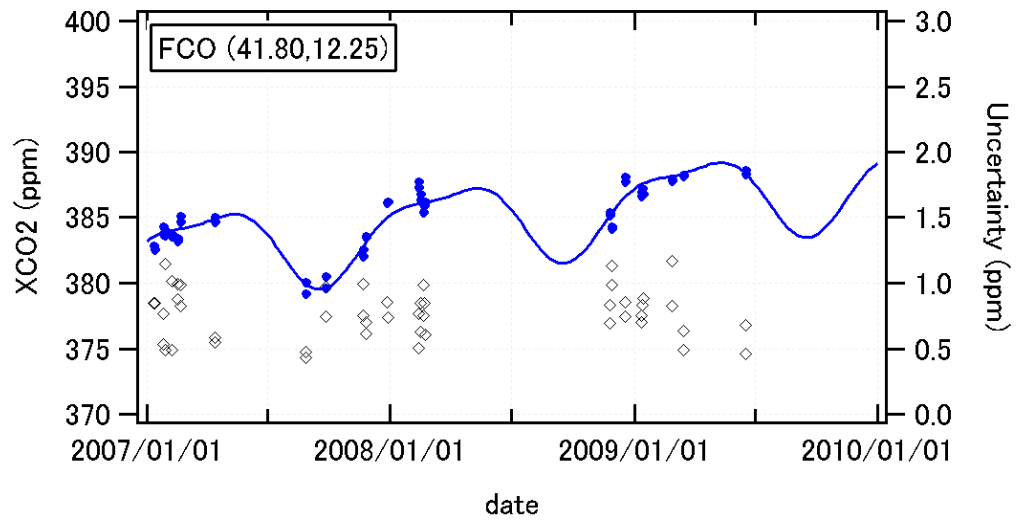
Supplementary materials for “Atmospheric column-averaged mole fractions of carbon dioxide at 53 aircraft measurement sites”.

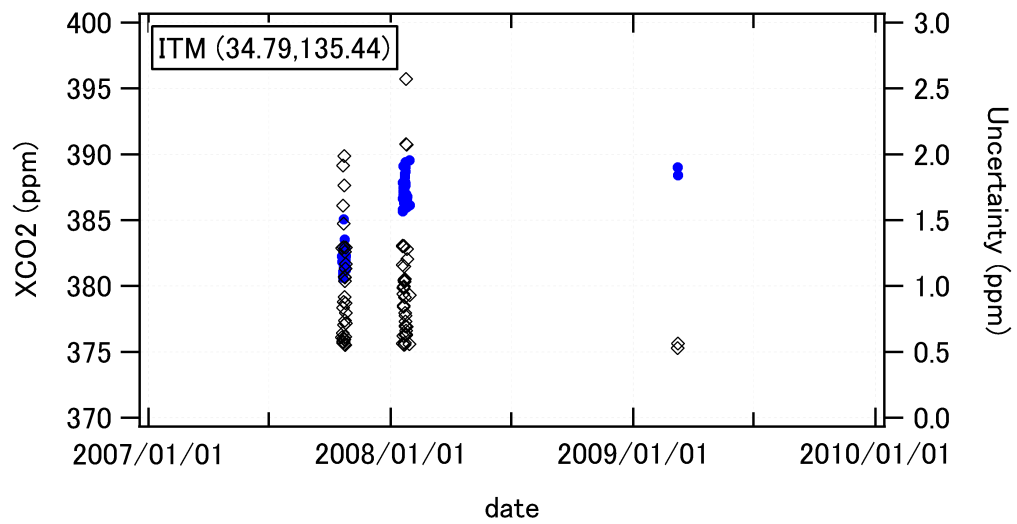
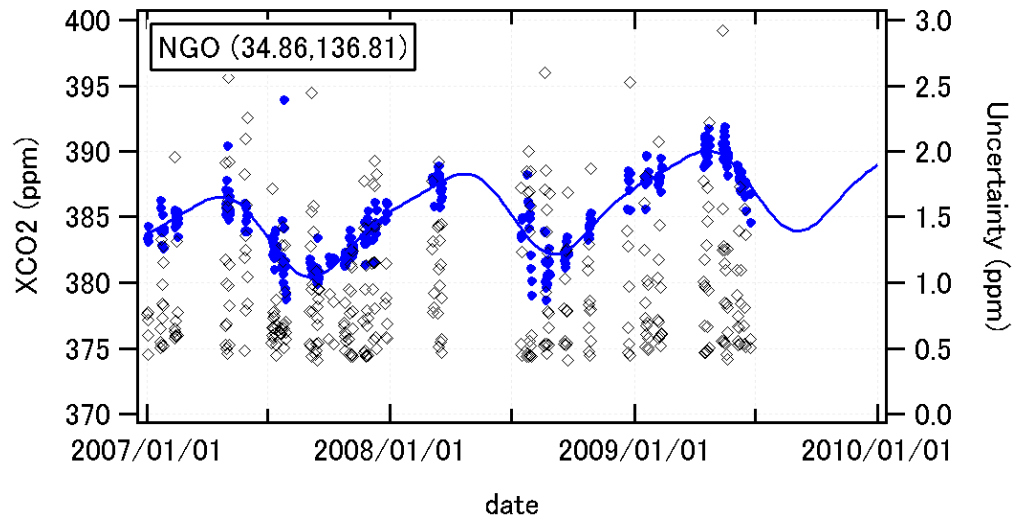
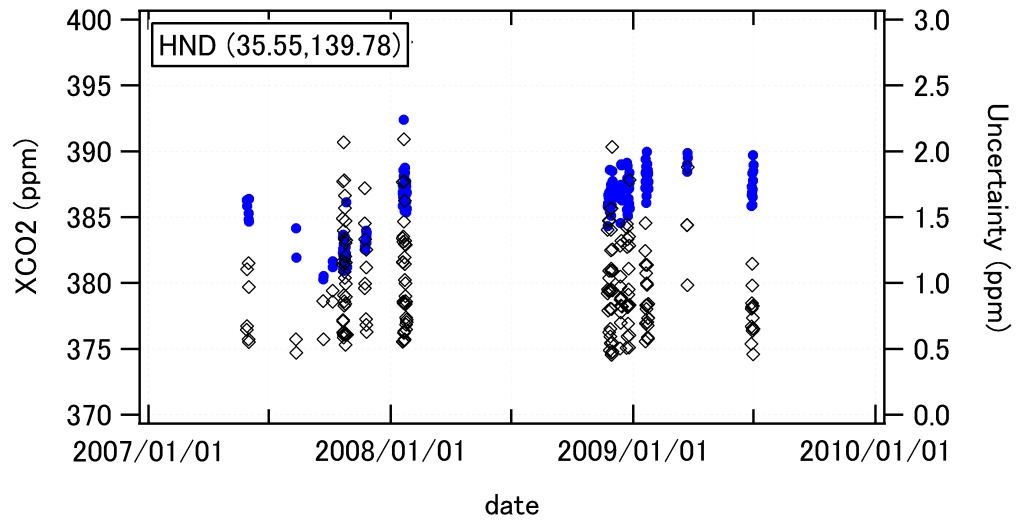
Y. Miyamoto, M. Inoue, I. Morino, O. Uchino, T. Yokota, T. Machida, Y. Sawa, H. Matsueda, C. Sweeney, P. P. Tans, A. E. Andrews, P. K. Patra

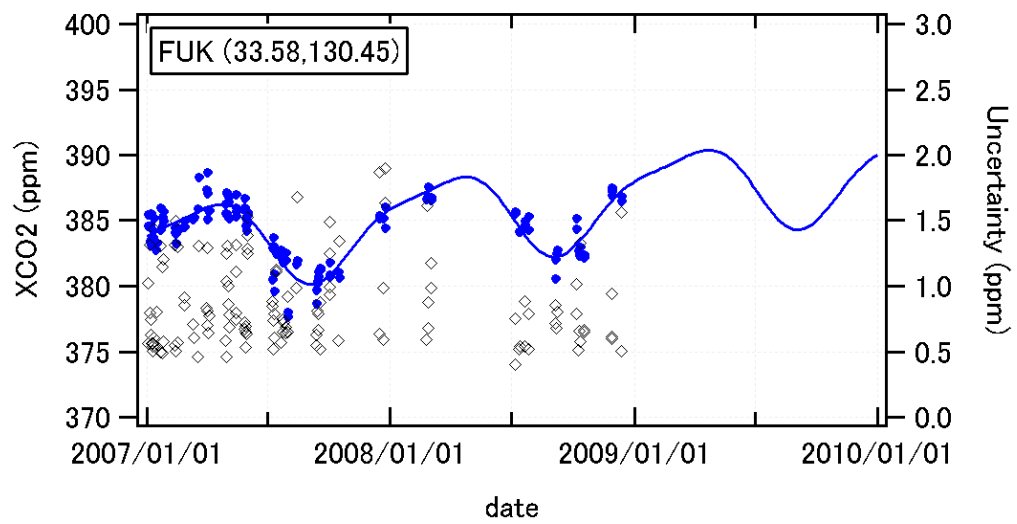
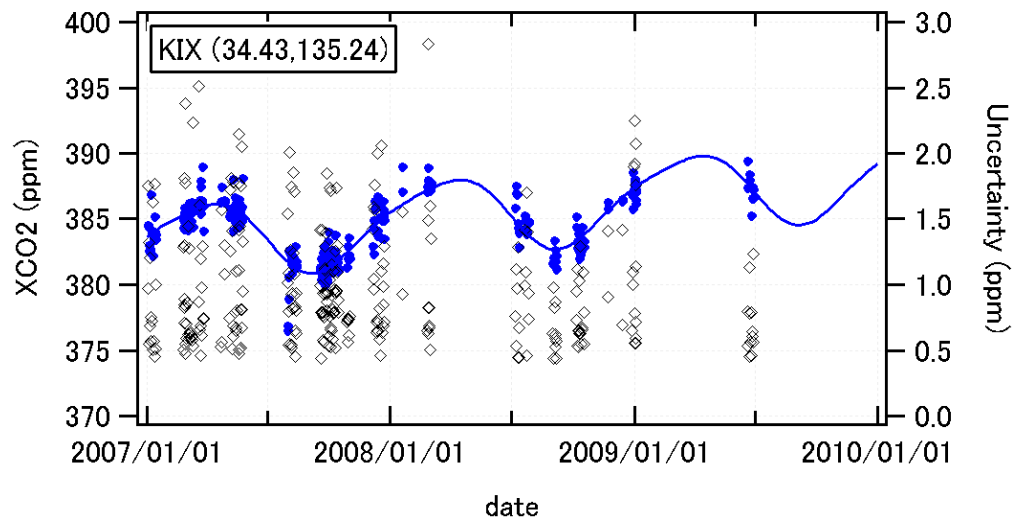
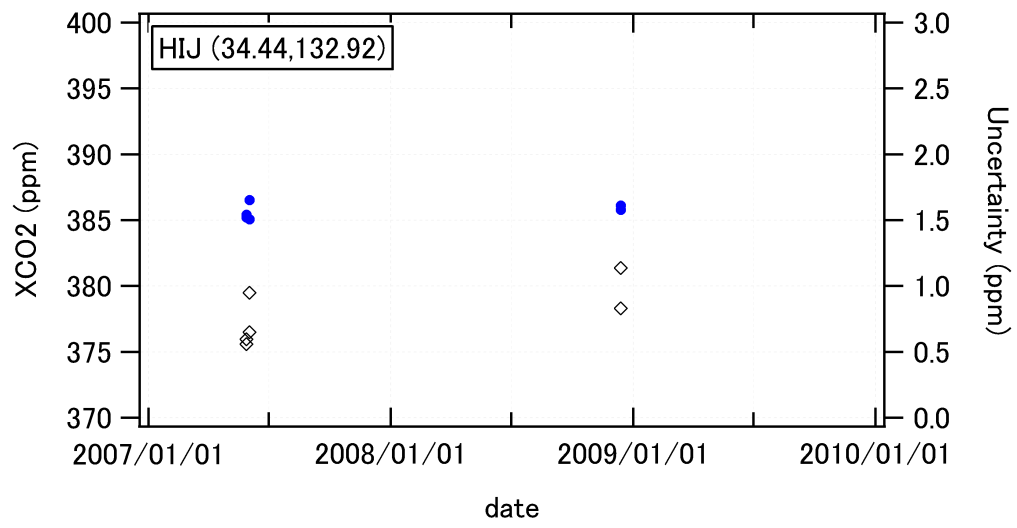
In Sect. 4 (Results and Discussion), we show the calculated XCO_2 values and their uncertainties at typical 7 sites in Fig. 4. Here, results for all the 53 sites are shown in Fig. A-1 (CONTRAIL sites), A-2 (NOAA sites) and A-3 (NIES sites). For convenience, results for the 7 sites remain in the figures.

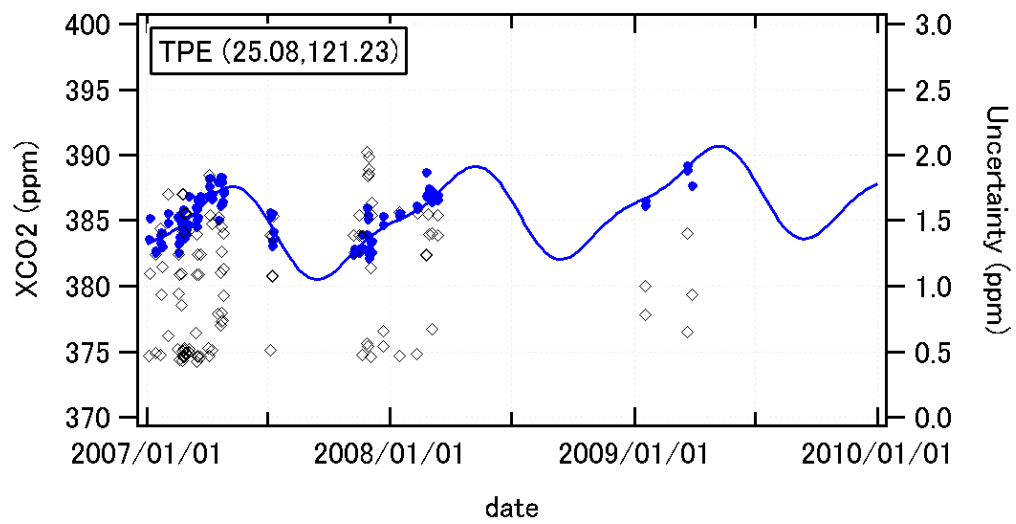
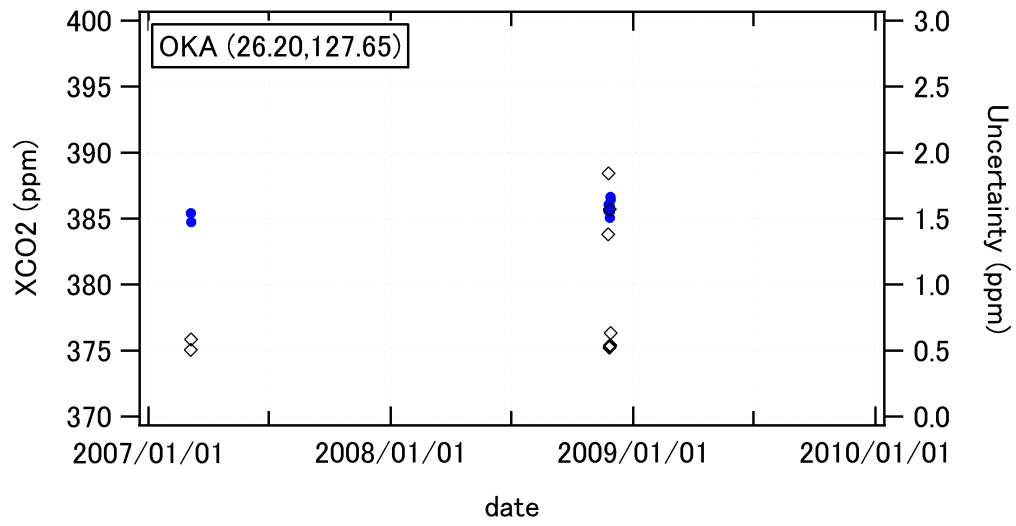
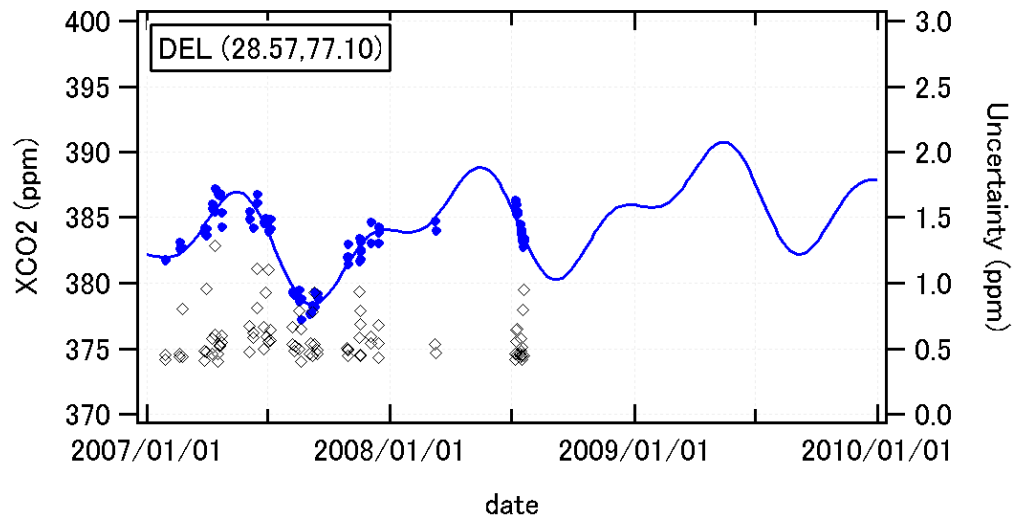


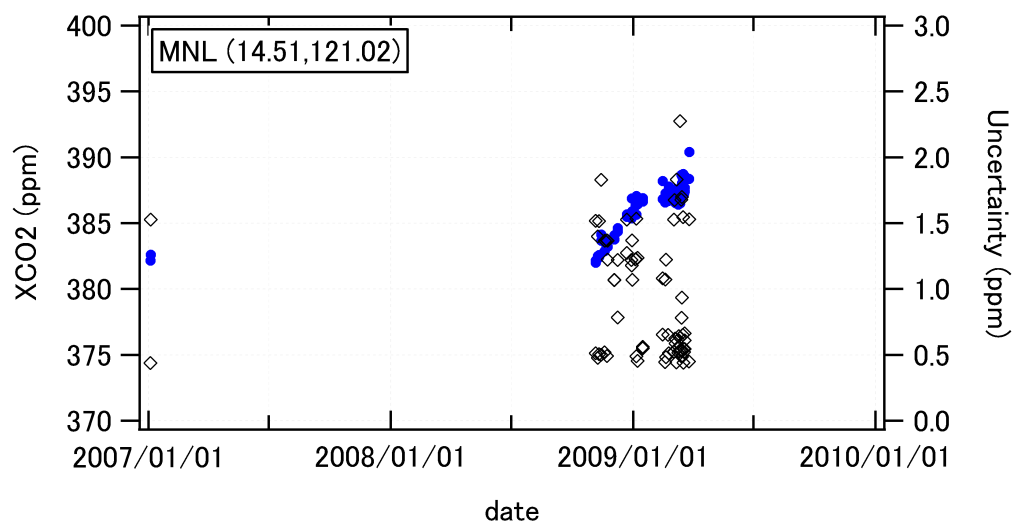
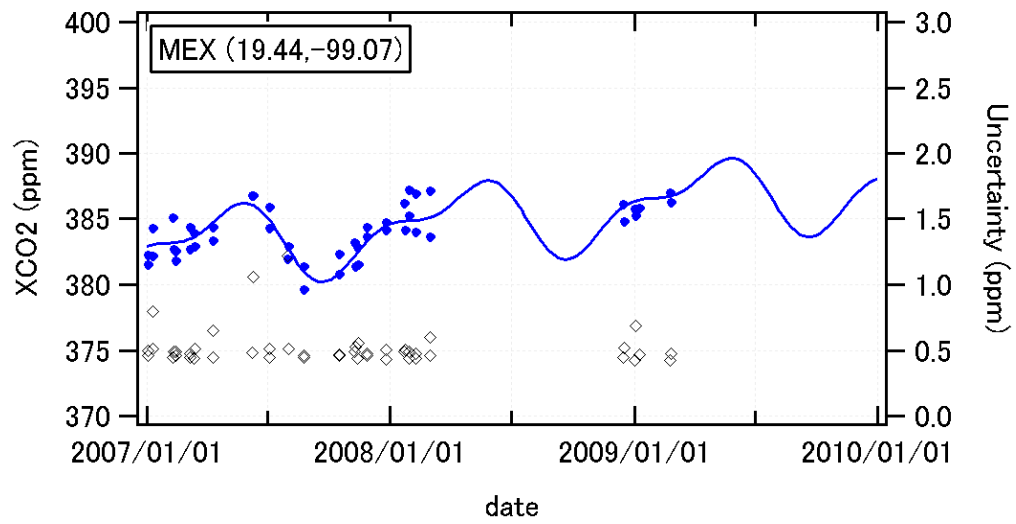
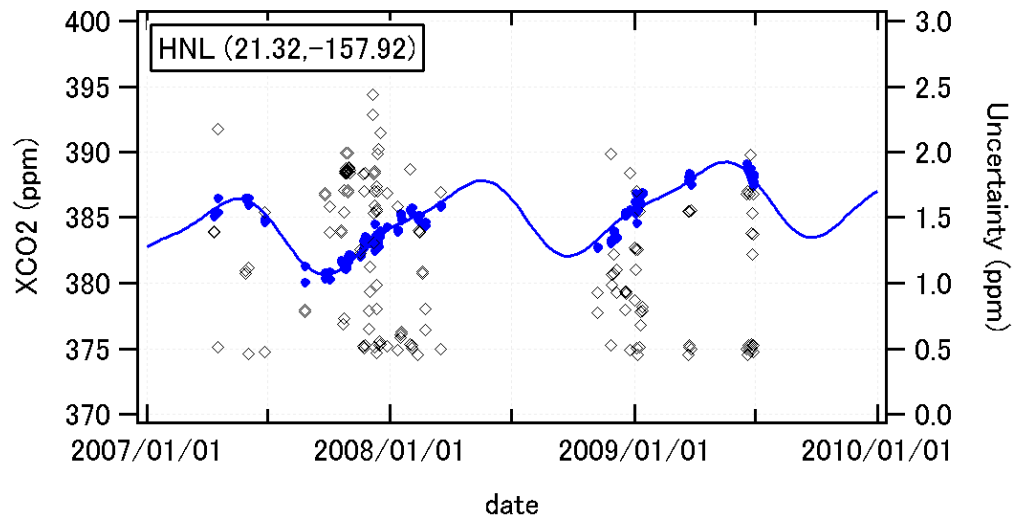


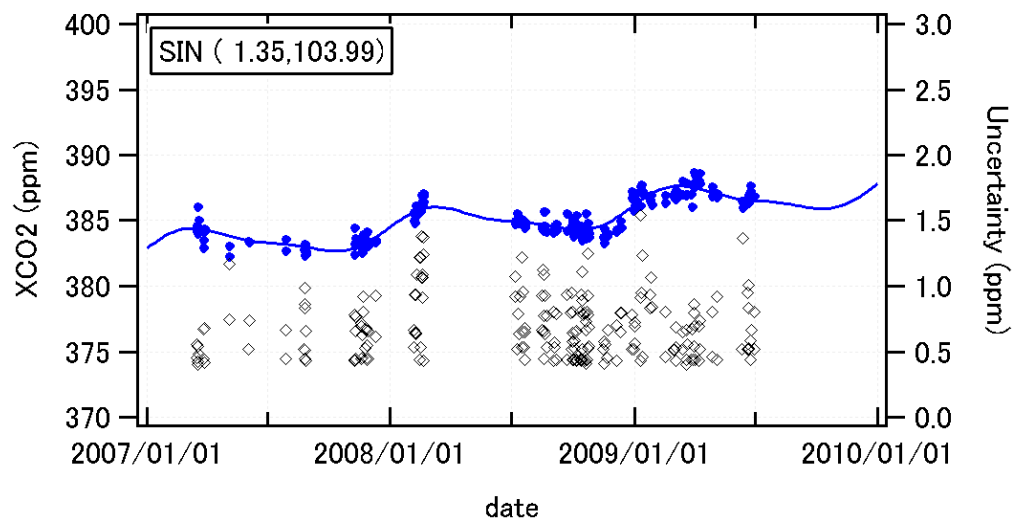
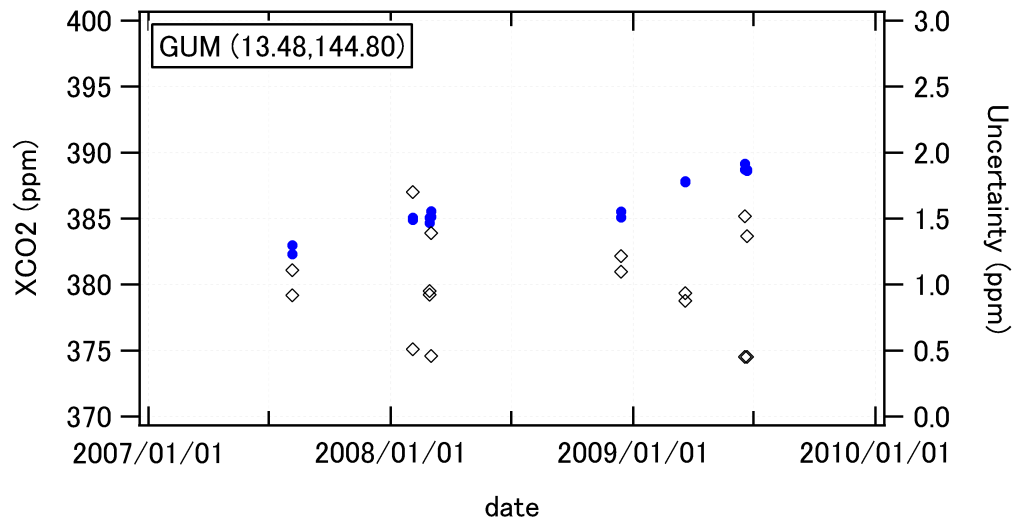
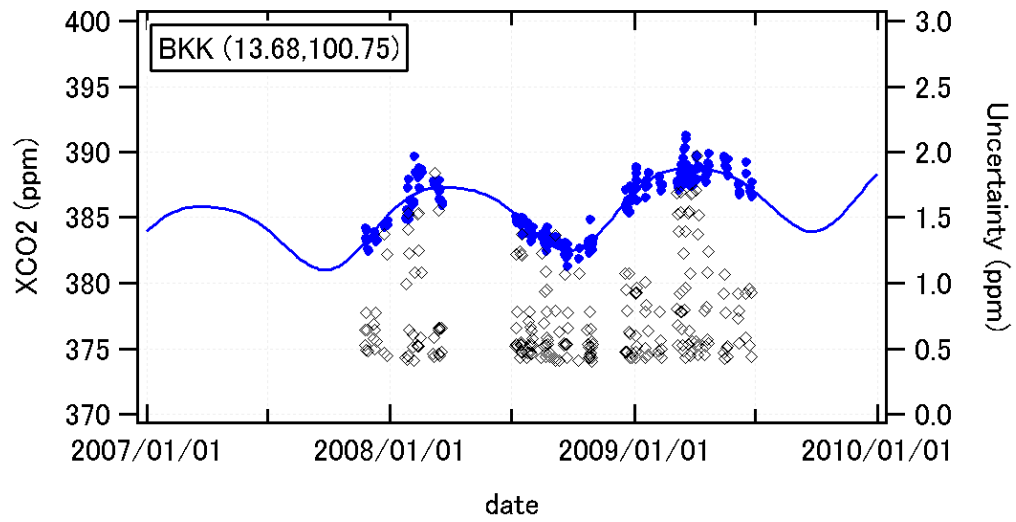


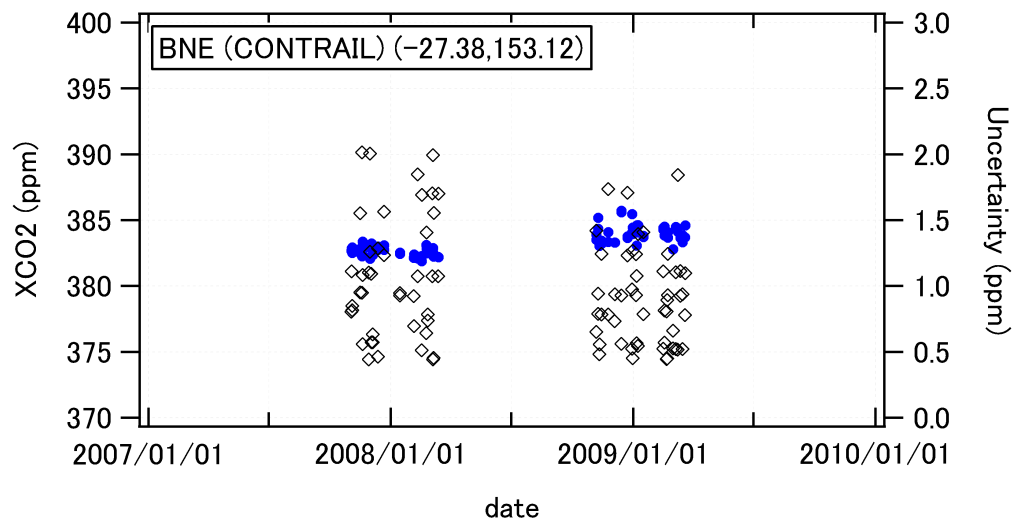
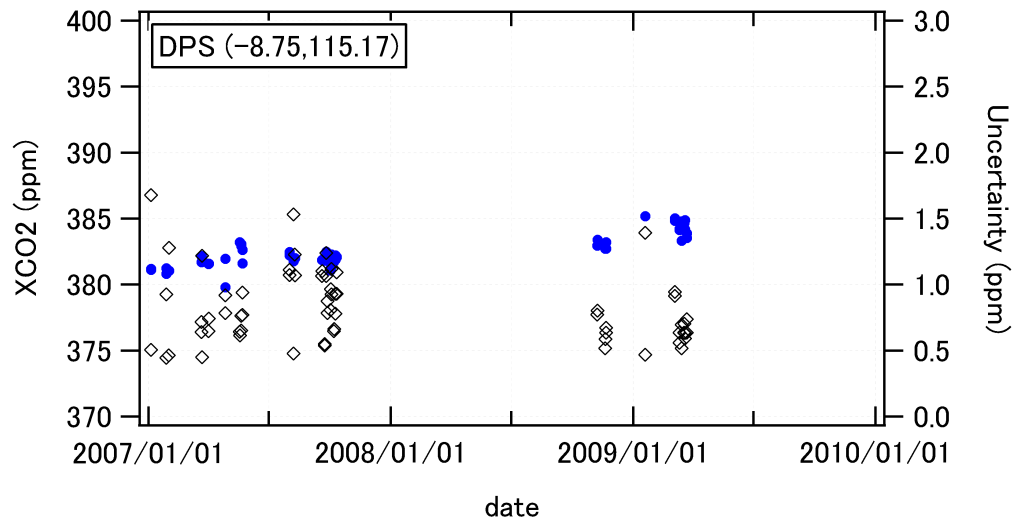
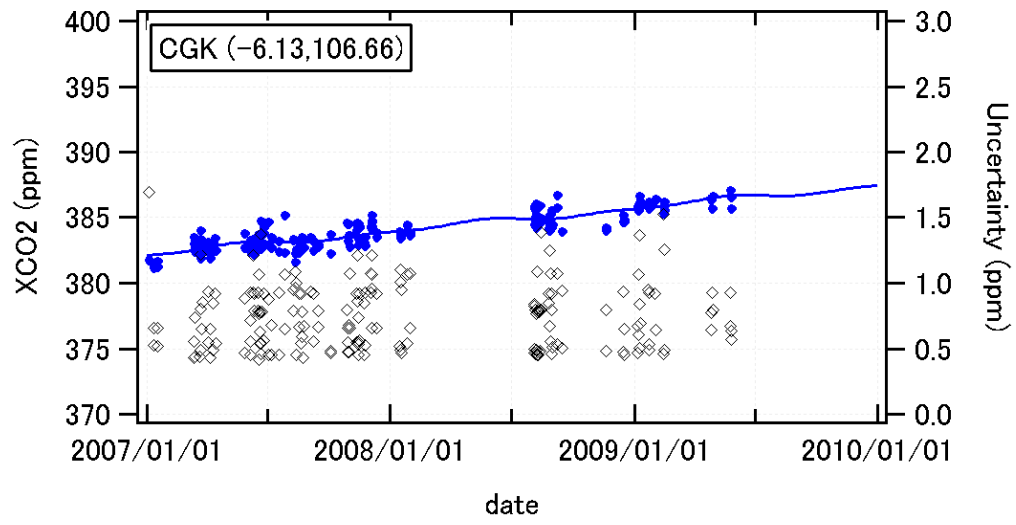












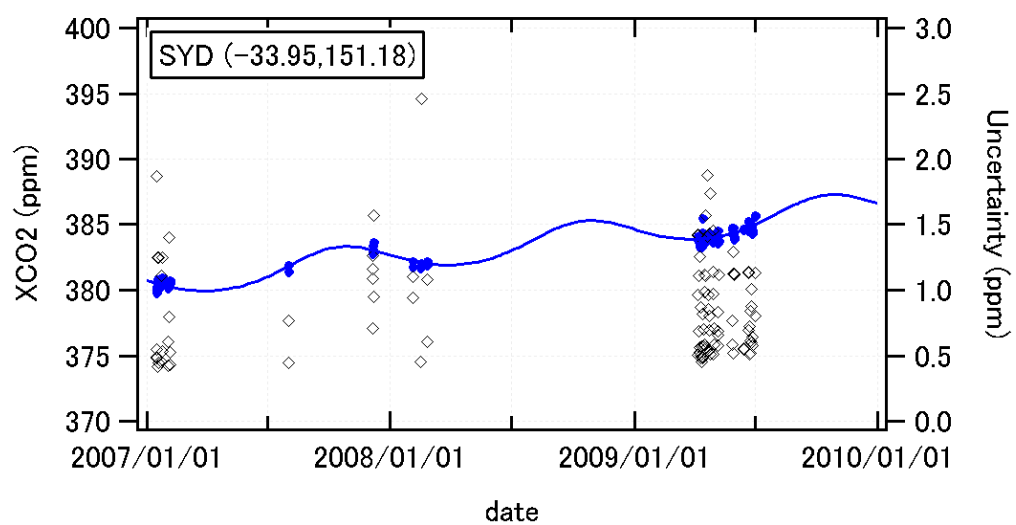
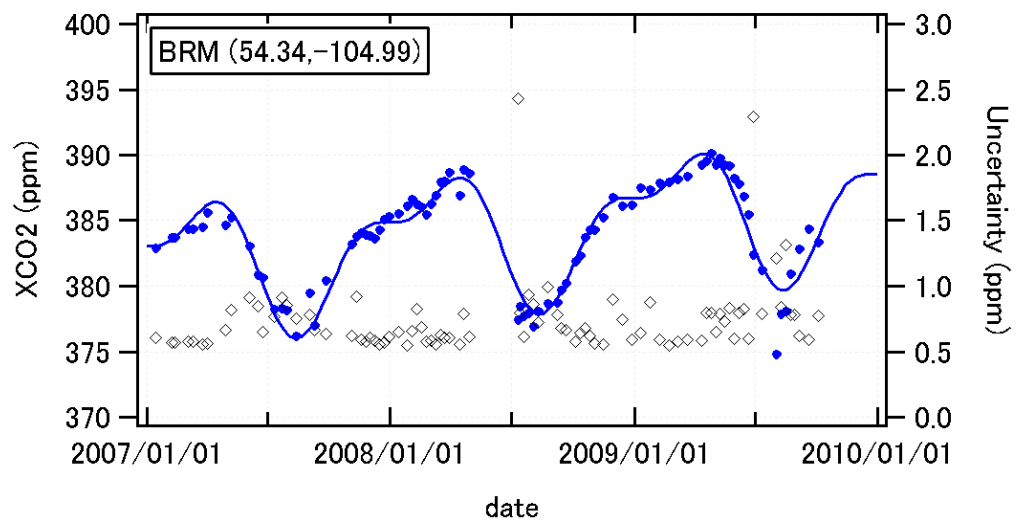
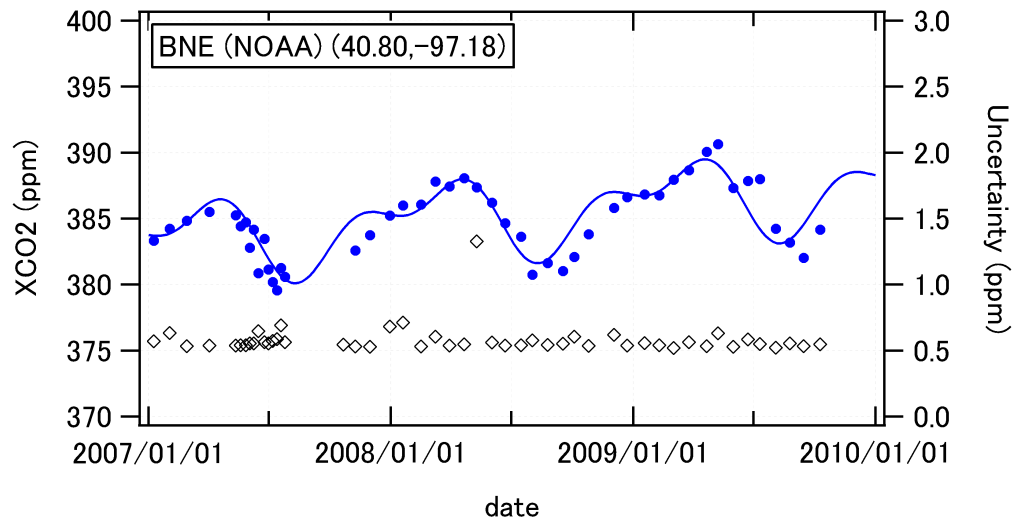
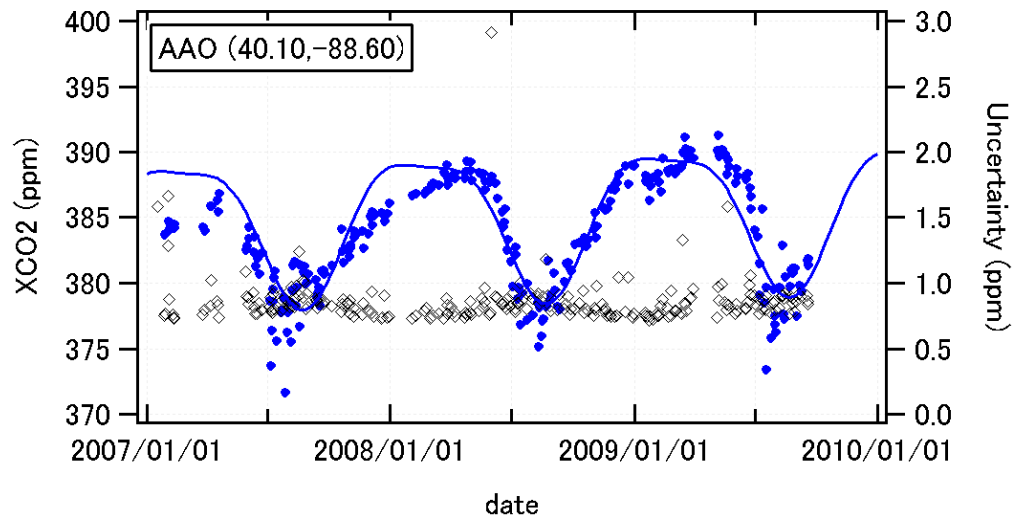
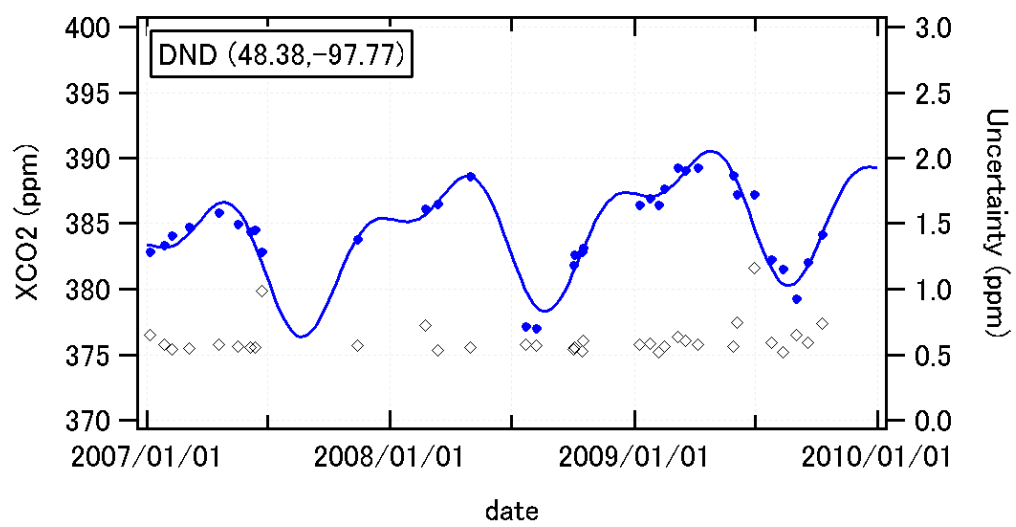
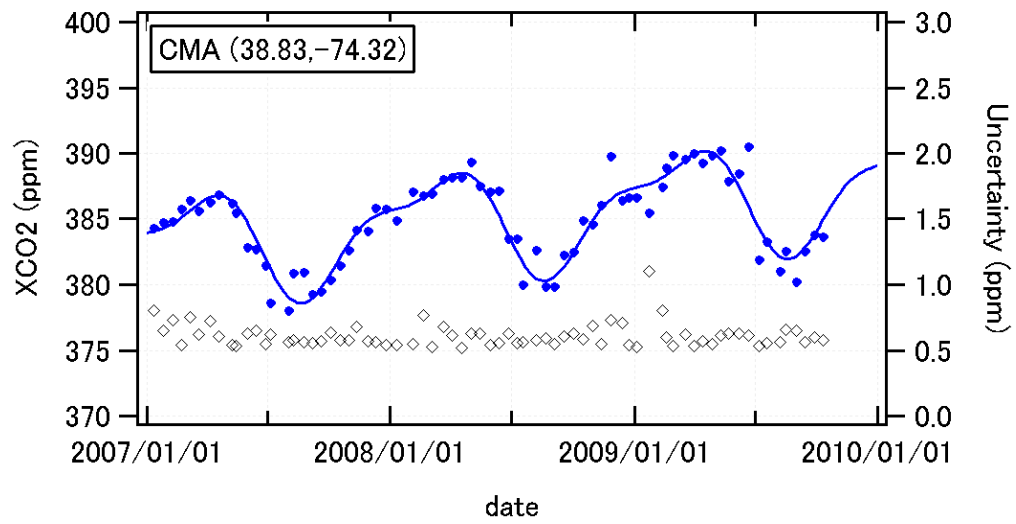
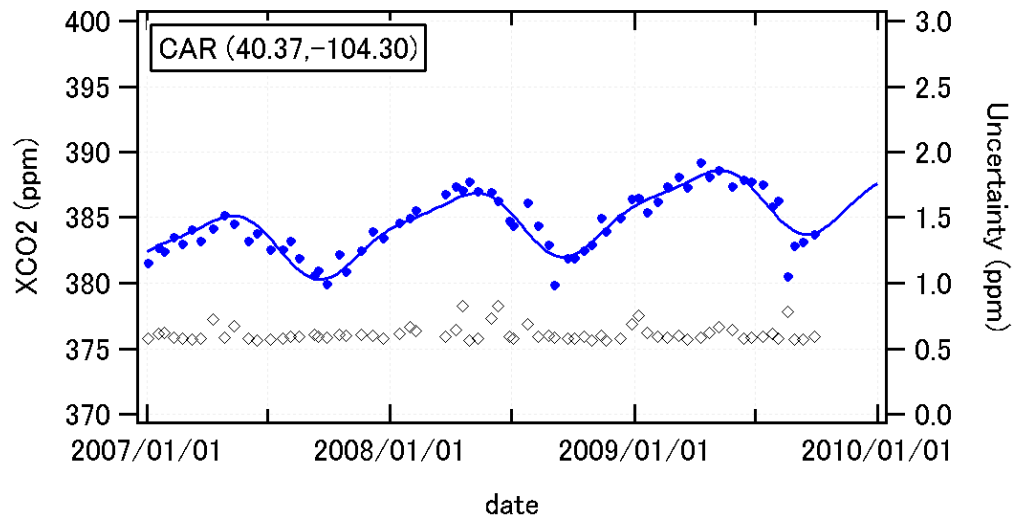
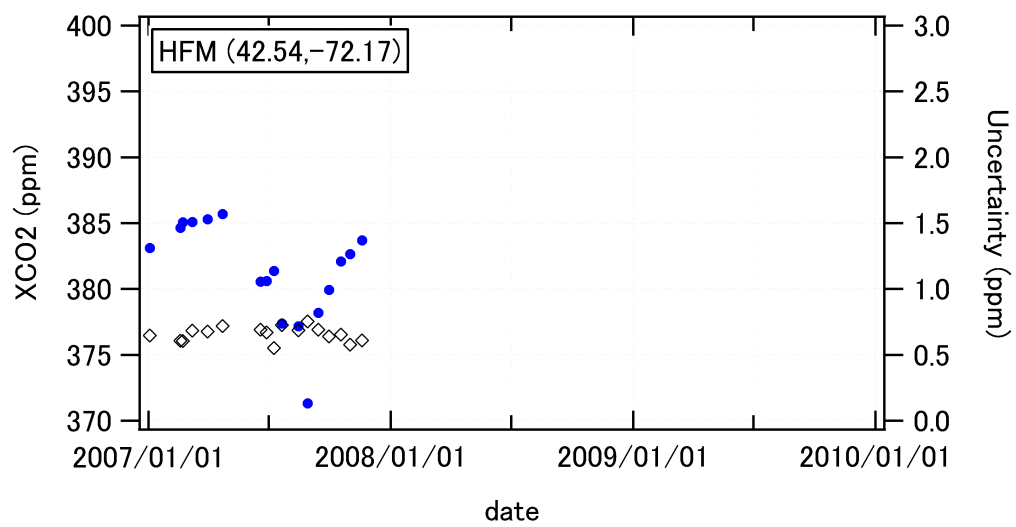
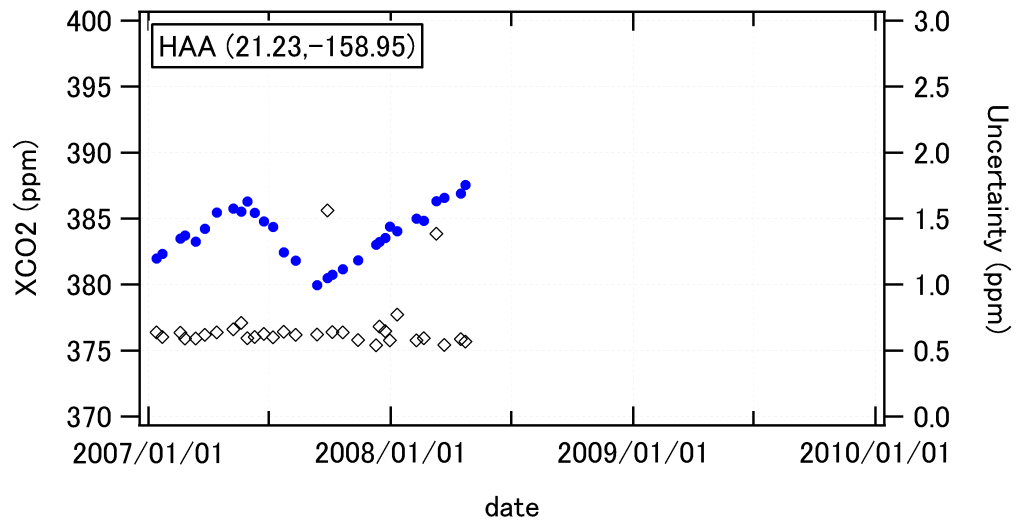
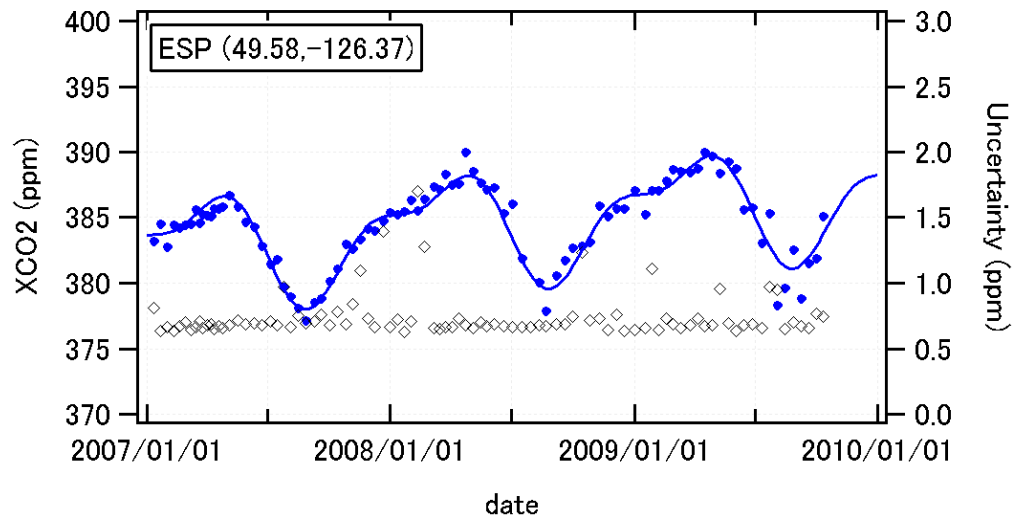
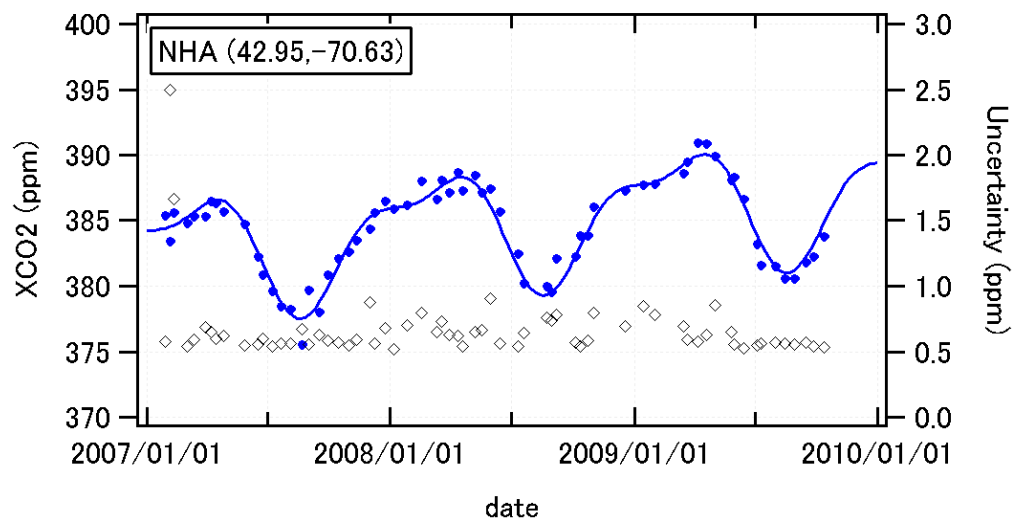
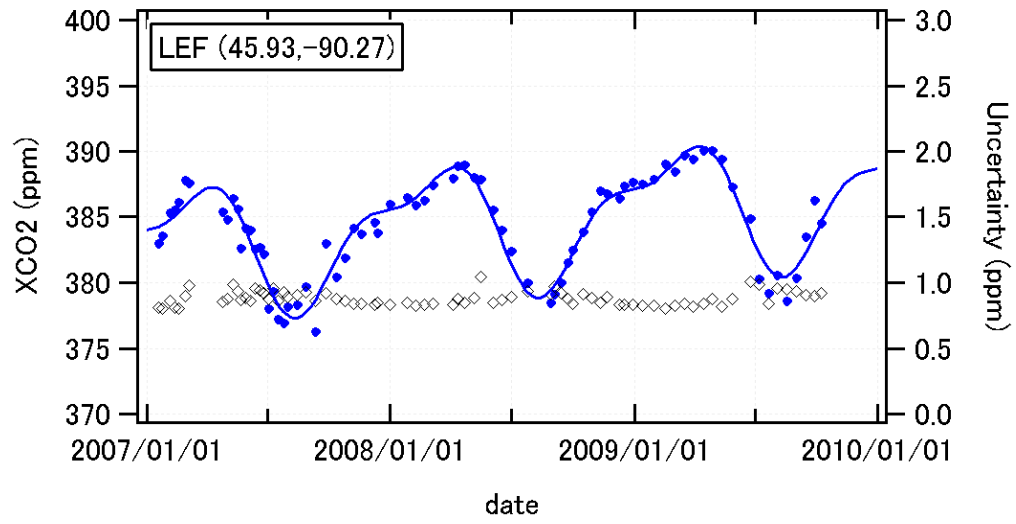
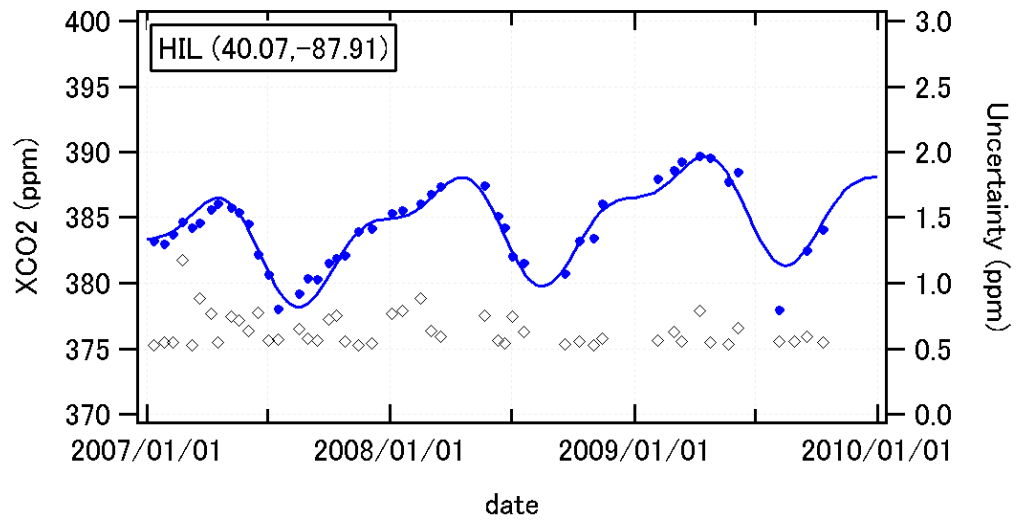


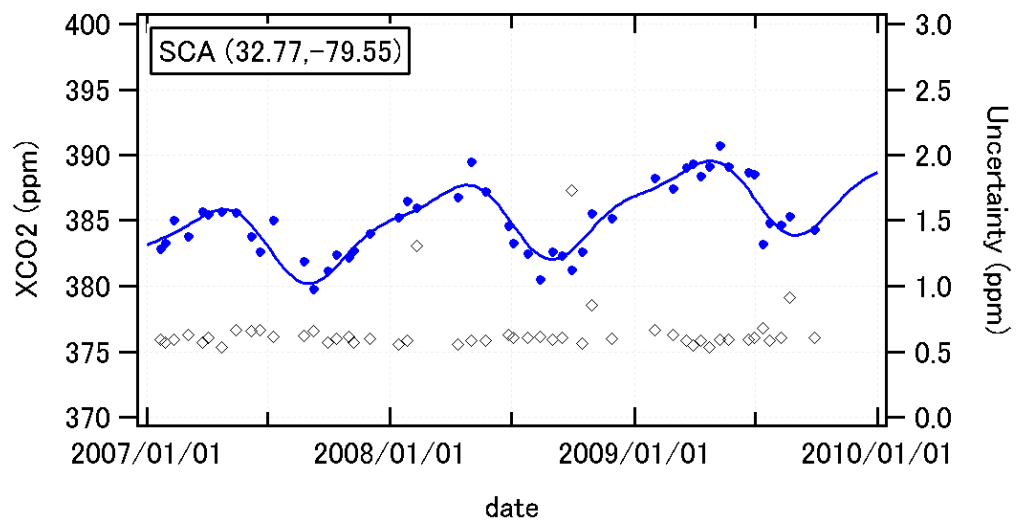
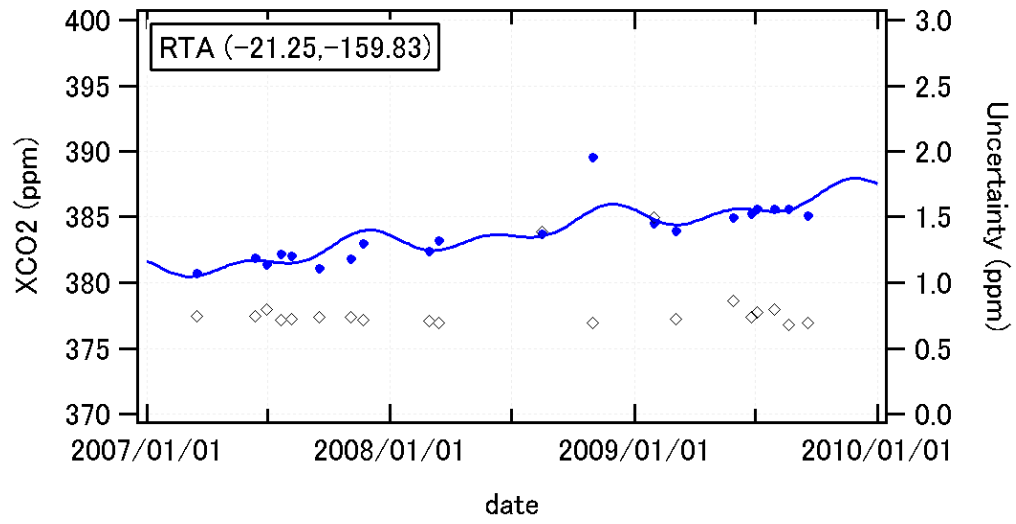
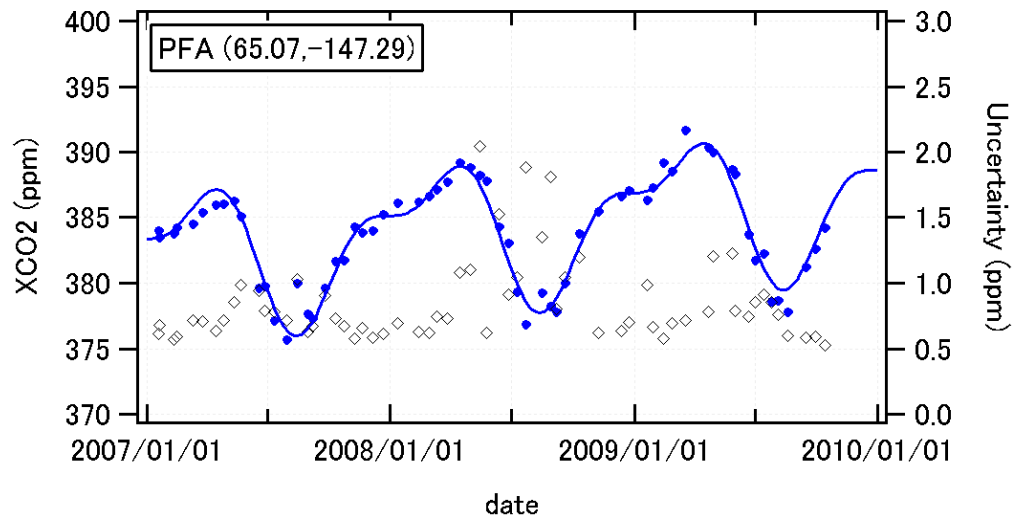
Figure A-1. Calculated XCO₂ values and their estimated uncertainties at the CONTRAIL sites. The site code (Table 1) and its latitude and longitude are shown at the upper left corner of each panel. Blue filled circles show XCO₂ (left axis), and black open rhomboids show their uncertainties (right axis). Blue solid lines show curves fitted to the temporal behavior of XCO₂ as a visual guide (only for sites where the number of data was sufficient).

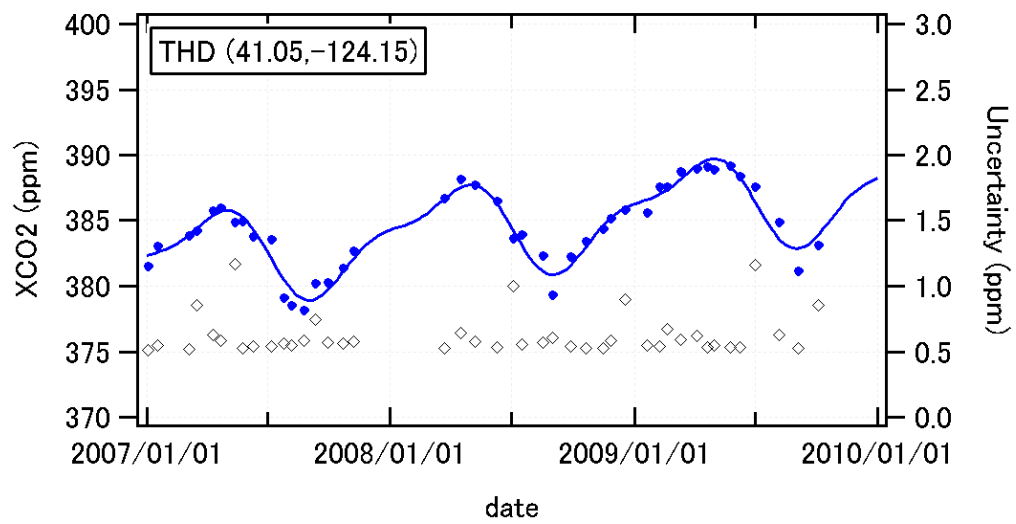
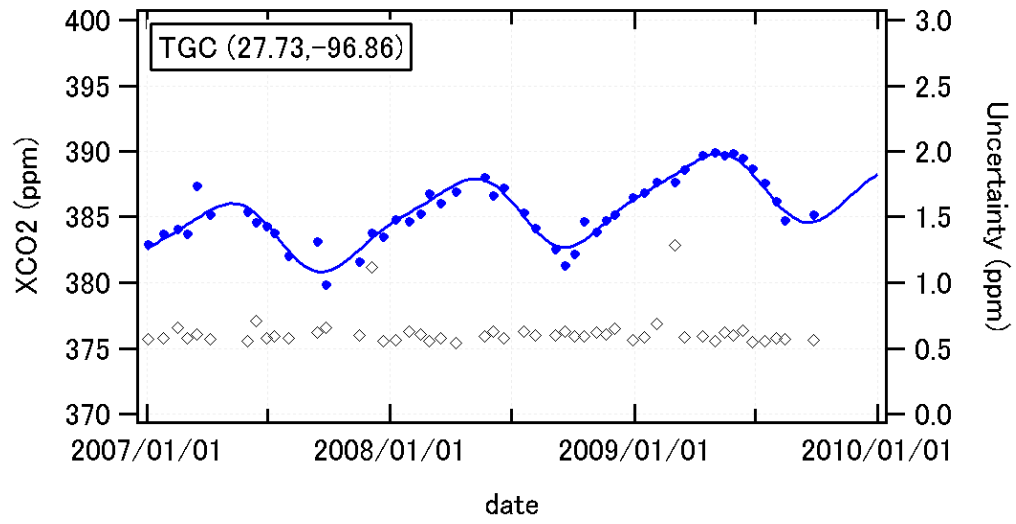
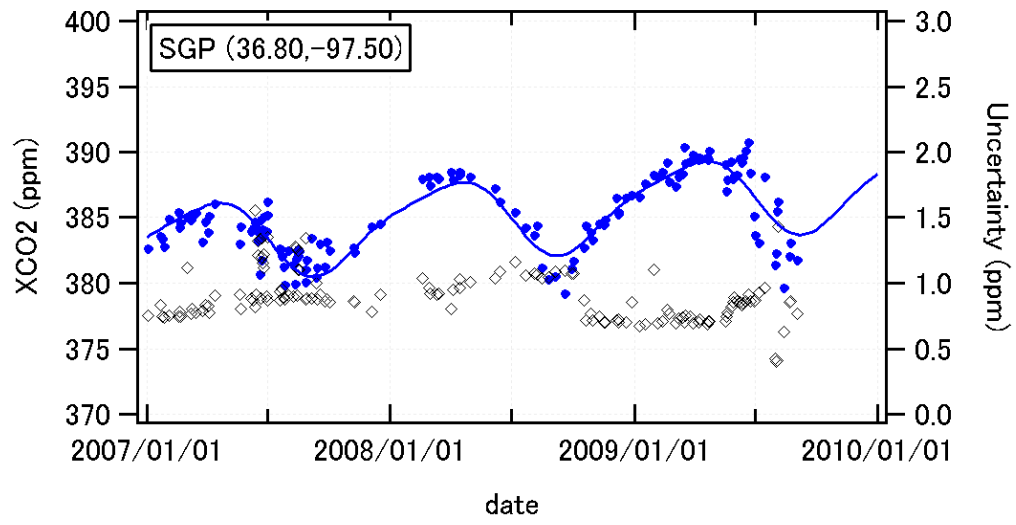












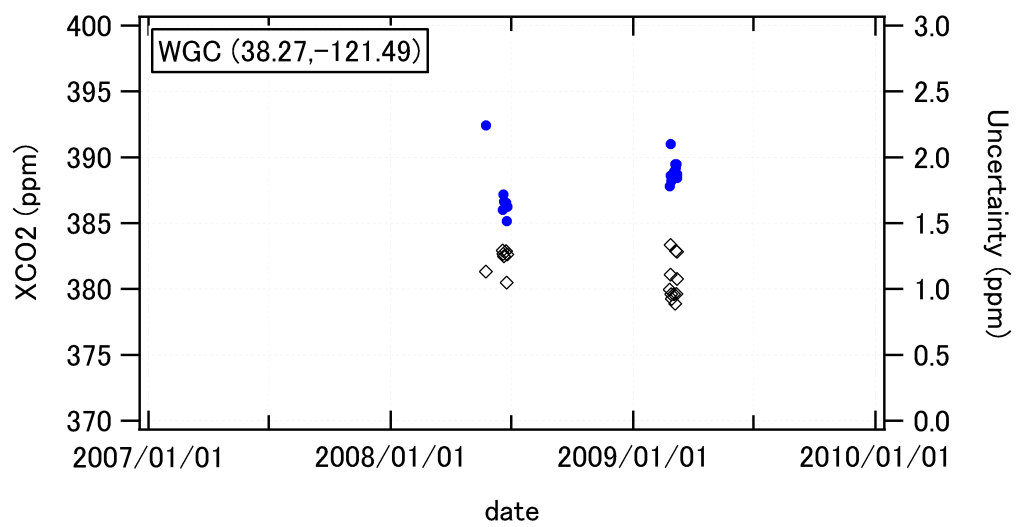
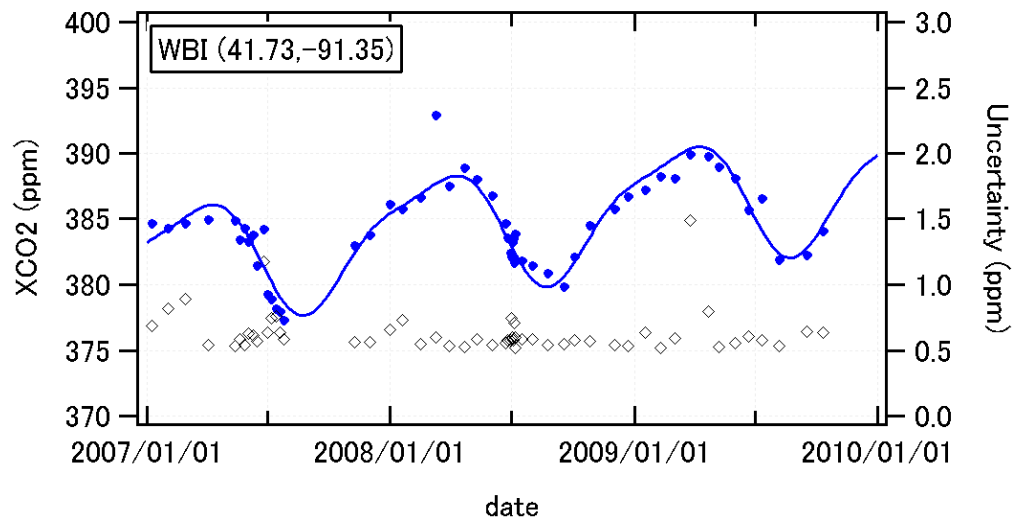
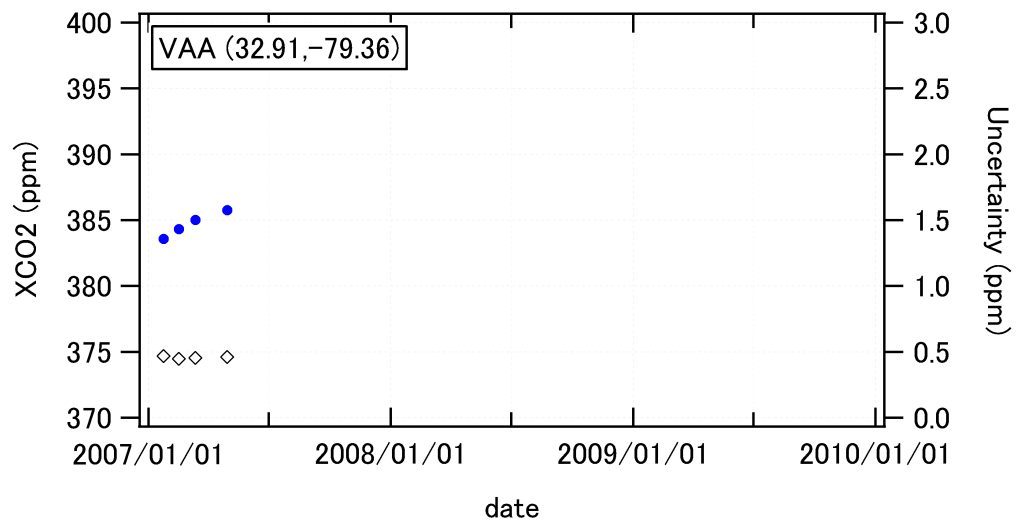
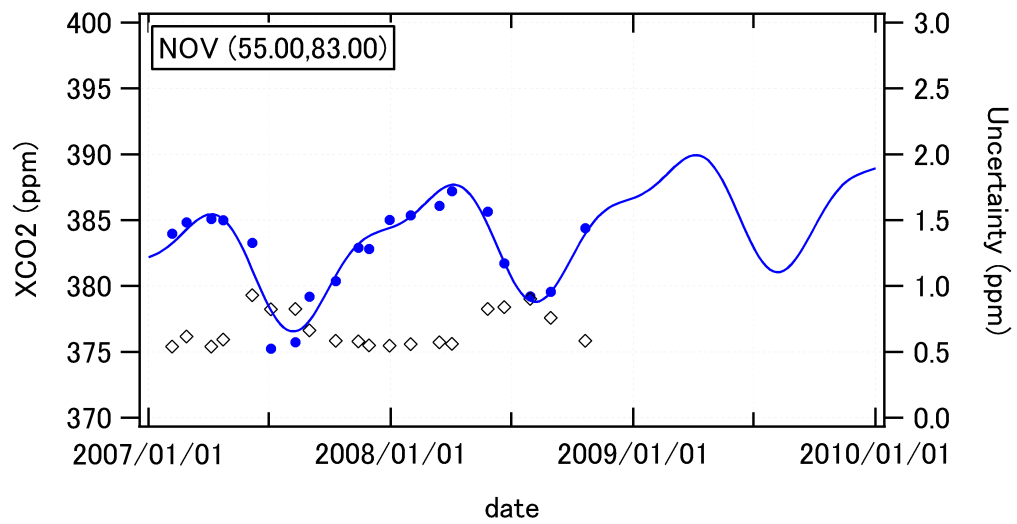
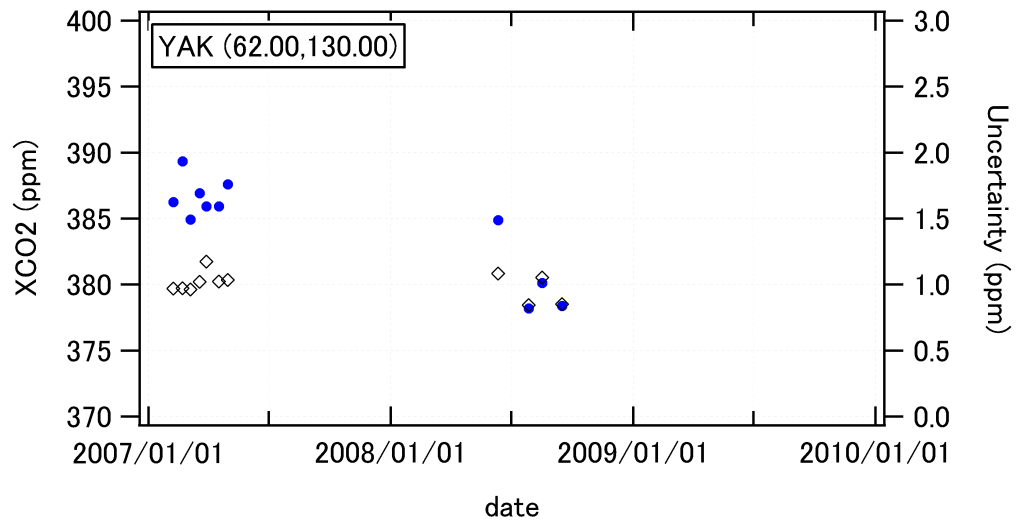
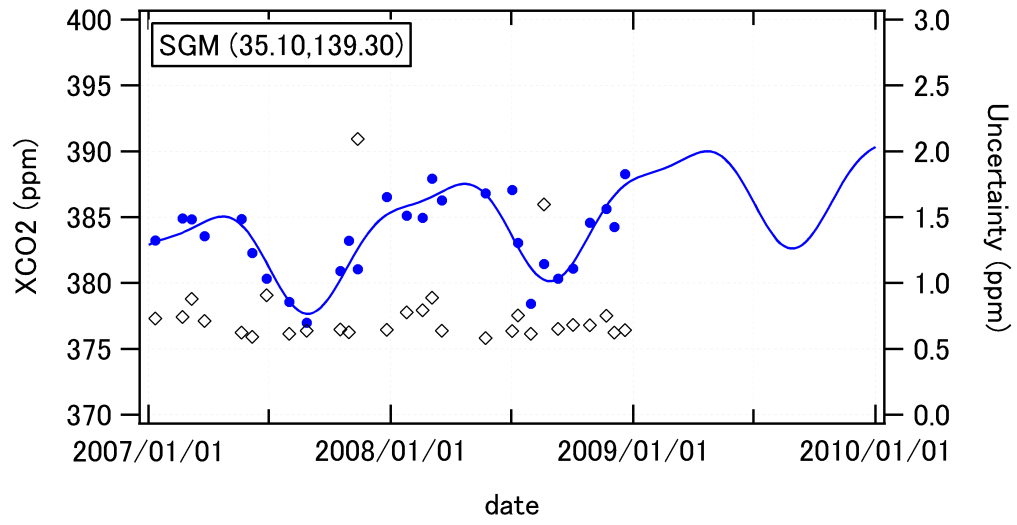


Figure A-2. Same as Fig. A-1 but showing the results at the NOAA sites.



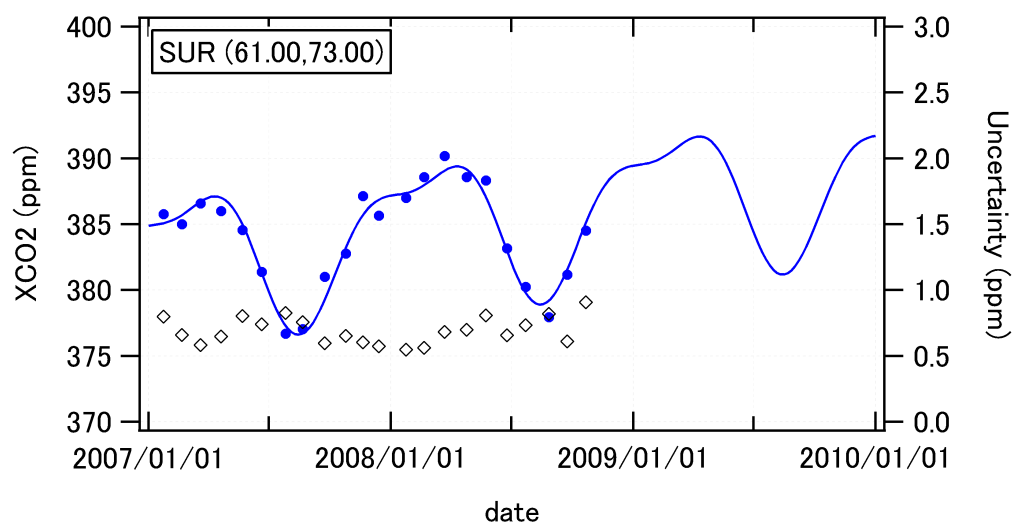


Figure A-3. Same as Fig. A-1 but showing the results at the NIES sites.